1969

Piezoelectric and elastic surface waves on LiNbOâ^'b3â^'s

Ronald Neil Spaight
Iowa State University

PIEZOELECTRIC AND ELASTIC SURFACE WAVES ON $LiNbO_3$

by

Ronald Neil Spaight

A Dissertation Submitted to the
Graduate Faculty in Partial Fulfillment of
The Requirements for the Degree of
DOCTOR OF PHILOSOPHY

Major Subject: Electrical Engineering

Approved:

Signature was redacted for privacy.
In Charge of Major Work

Signature was redacted for privacy.
Head of Major Department

Signature was redacted for privacy.
Dean of Graduate College

Iowa State University
Of Science and Technology
Ames, Iowa

1969

TABLE OF CONTENTS

I. INTRODUCTION

The first investigation of surface waves was reported by Lord Rayleigh (9) in 1885. This investigation discussed waves on the surface of a semi-infinite, isotropic, perfectly elastic body. These waves were characterized by exponential decay of the displacement amplitude with increasing distance from the surface. The displacements form a retrograde ellipse in a plane normal to the surface and parallel to the direction of propagation. This plane is referred to as the sagittal plane and the propagation mode as a Rayleigh wave. The decay constants of this wave give exponential decay away from the surface and propagational parallel to it.

In 1911 Love (6) discussed a different type of surface wave. Propagation of this wave takes place in a layer of isotropic material of infinite length resting on a different semi-infinite isotropic medium. This mode occurs only if the velocity of the shear waves in the layer is less than the velocity of shear waves in the substrate. The particle motion of this mode is simpler than the Rayleigh mode in that the displacement is parallel to the wave fronts and to the surface. It differs from a bulk shear wave in that the amplitude decreases exponentially away from the surface. This mode is referred to as a Love wave. One important distinction between Love and Rayleigh waves is the frequency dependence of the propagation velocity; Rayleigh wave velocity

is independent of frequency while Love waves are frequency dependent.

Surface waves in anisotropic materials were considered by Stoneley (10) in 1955 for crystals of cubic symmetry. Rayleigh waves were found to exist for certain values of C_{11}, C_{12}, and C_{44}, the elastic rigidity constants, over a (0,0,1) surface of a cubic crystal and not for others. For the values of C_{11}, C_{12}, and C_{44} which do not allow Rayleigh waves a real phase velocity associated with complex decay constants are found. These waves have displacements which attenuate as a product of an exponential function and a trigonometric function. Waves of this type are referred to as generalized Rayleigh waves. Stoneley also demonstrated that Love waves can exist only in two symmetrical cases; when Love waves exist the generalized Rayleigh wave degenerates to a superposition of Rayleigh and Love waves.

Gold (4) and Derewsiewicz and Mindlin (2) have reported work on surface waves in cubic and monoclinic crystals respectively. In 1957 Synge (12) presented a formal treatment of various types of surface waves in anisotropic material and found that for certain values of the elastic constants propagation in certain directions was not allowed. Gazis, Herman and Wallis (3) determined the range of elastic constants for which Rayleigh waves exist on a (100) free surface in cubic crystals. They also found the generalized Rayleigh wave for other ranges of elastic constants.

Neither Rayleigh nor generalized Rayleigh-waves may be possible in certain directions parallel to a free surface, depending on the values of the elastic constants.

White (17) and Tseng and White (15) investigated the possibility of surface wave propagation on the free surface of the basal plane of hexagonal piezoelectric crystals. They concluded that two uncoupled modes were possible, the Rayleigh wave and an uncoupled transverse mode, but only the Rayleigh wave solution would allow boundary conditions to be matched. Complete solutions for the Rayleigh wave were calculated. Tseng (13) extended the analysis to metalized surfaces of the same class of crystals.

Koerber (5) demonstrated that piezoelectric surface waves decouple to form independent Rayleigh and transverse modes if they are uniform in a direction perpendicular to the sagittal plane and parallel to a plane of symmetry or perpendicular to a two-fold axis of symmetry. For the sagittal plane parallel to a plane of symmetry all field and displacement components are coplanar for a particular mode, while field and displacements are mutually orthogonal for the sagittal plane perpendicular to a two-fold axis.

In recent years a great deal of interest in surface wave propagation as a method of obtaining high frequency (100 MHz - 1 GHz) delay lines at relatively low loss has been created due to the development of the technical ability to fabricate interdigital transducers. These

transducers (see White and Voltmer (18)) are highly efficient and provide a direct electromagnetic to acoustic energy conversion. More will be said about these transducers later. Several materials have been used as substrates for surface wave propagation. Among the most popular are cadmium sulfide, CdS, and lithium metaniobate, $LiNbO_3$. CdS is of hexagonal symmetry and has been theoretically analyzed by Tseng and White.

The variation of phase velocity with propagation direction on X-cut and Y-cut crystals of $LiNbO_3$ was reported by Campbell and Jones (1) in 1968. They investigated the change in phase velocity for a metalized and free surface. An electrostatic approximation was used and displacement and potential curves were given for certain directions of propagation.

For propagation on Y-cut crystals along the trigonal axis in $LiNbO_3$ the piezoelectric surface waves decouple into two independent modes. These modes are referred to as the transverse and Rayleigh modes. Campbell and Jones (1) did not report the displacement or field behavior for this particular direction of propagation where decoupling occurs. To obtain detailed information of the variation of the electromagnetic fields inside the crystal Maxwell's equations must be solved together with the stress equations of motion.

It is the purpose of this dissertation to theoretically investigate surface wave propagation on trigonal crystals,

$LiNbO_3$ in particular, and to verify the existence of such modes experimentally. A detailed solution giving plots for variations of fields and displacements as a function of distance from the free surface and experimental verification of propagation velocity are the main goals of this work.

II. THEORETICAL DEVELOPMENT

Newton's second law of motion requires elastic wave propagation to obey the equation of motion given by

$$\rho \frac{\partial^2 u_i}{\partial t^2} = \frac{\partial T_{ij}}{\partial x_j} , \tag{1}$$

where ρ is the density of the crystal,

u_i is the particle displacement in cartesian coordinates x_i,

T_{ij} is the second rank stress tensor.

For nonpiezoelectric crystals the stress tensor of Equation 1 is given by Hooke's law as

$$T_{ij} = C_{ijkl} S_{kl} \tag{2}$$

where S_{kl} is a second rank strain tensor,

C_{ijkl} is a fourth rank tensor of elastic rigidity constants at constant entropy.

The strain tensor is related to the displacements, u_i, by

$$S_{kl} = \frac{1}{2}\left(\frac{\partial u_k}{\partial x_l} + \frac{\partial u_l}{\partial x_k}\right) . \tag{3}$$

Elastic wave propagation for nonpiezoelectric crystals can be summarized as a solution to the equations of motion

4 $$\frac{\partial^2 u_i}{\partial t^2} = \frac{1}{2} C_{ijkl} \left(\frac{\partial u_k}{\partial x_l} + \frac{\partial u_l}{\partial x_k}\right)$$

subject to the boundary conditions that the surface of propagation is stress free, i.e. the normal components of the stress vector[1] vanish at the surface.

Propagation on piezoelectric crystals is usually complicated by the presence of a piezoelectric surface wave which contains electromagnetic field quantities. These field quantities must satisfy Maxwell's equations for a magnetically isotropic dielectric,

5a $$\frac{\partial D_i}{\partial x_i} = 0,$$

5b $$\frac{\partial H_j}{\partial x_j} = 0,$$

5c $$\varepsilon_{ijk} \frac{\partial H_k}{\partial x_j} = \frac{\partial D_i}{\partial t},$$

5d $$\varepsilon_{ijk} \frac{\partial E_k}{\partial x_j} = - \mu_0 \frac{\partial H_i}{\partial t},$$

where D_i is the electric flux density,

H_j is the magnetic field intensity,

μ_0 is the permeability of free space,

ε_{ijk} is the rotation tensor.

---

[1] The stress vector is the vector obtained by contracting the stress tensor with a unit vector normal to a surface.

A combination of Equations 5c and 5d which eliminates the magnetic field, H_i, is of particular use here,

$$6 \qquad \frac{\partial E_j}{\partial x_i \partial x_j} - \frac{\partial E_i}{\partial x_j \partial x_j} = -\mu_0 \frac{\partial^2 D_i}{\partial t^2} \quad .$$

Due to the presence of the electric field in piezoelectric materials the stress tensor contains an additional term relating stresses to electric fields. The stress tensor for piezoelectric crystals becomes

$$7 \qquad T_{ij} = C_{ijkl} S_{kl} - e_{pij} E_p$$

where e_{pij} is a third rank tensor of piezoelectric constants. Components of the electric flux density are given by

$$8 \qquad D_i = e_{ikl} S_{kl} + \varepsilon_{ip} E_p$$

where ε_{ip} is the dielectric permittivity at constant strain.

Elastic and piezoelectric wave propagation for piezoelectric crystals can be summarized as a solution to the equations of motion, Equations 1, where T_{ij} is given by Equation 7 subject to the boundary conditions: 1) The surface of propagation is stress free, 2) The electromagnetic field components are appropriately matched across the surface.

For simplicity engineering notation as discussed by Mason (7) will now be employed to reduce the number of subscripts. Engineering notation allows designation of elastic constants by two subscripts, stress components by one, and similar reductions of other appropriate quantities. This notation makes the following substitutions,

Engineering notation	Tensor notation
1	11
2	22
3	33
4	23 = 32
5	13 = 31
6	12 = 21.

For example C_{1122} becomes C_{12}, and T_{13} becomes T_5.

Symmetry of crystals of the trigonal class C_{3v} (point group 3m) reduces the stress components and electric flux density components of Equations 7 and 8 to

$$
\begin{aligned}
T_1 &= C_{11}S_1 + C_{12}S_2 + C_{13}S_3 + C_{14}S_4 + e_{22}E_2 - e_{31}E_3 \\
T_2 &= C_{12}S_1 + C_{22}S_2 + C_{13}S_3 - C_{14}S_4 - e_{22}E_2 - e_{31}E_3 \\
T_3 &= C_{13}S_1 + C_{13}S_2 + C_{33}S_3 - e_{33}E_3 \qquad (9) \\
T_4 &= C_{14}S_1 - C_{14}S_2 + C_{44}S_4 - e_{15}E_2 \\
T_5 &= C_{44}S_5 + C_{14}S_6 - e_{15}E_1
\end{aligned}
$$

$$T_6 = C_{14}S_5 + C_{66}S_6 + e_{22}E_1$$

$$D_1 = e_{15}S_5 - e_{22}S_6 + \varepsilon_{11}E_1$$

9

$$D_2 = -e_{22}S_1 + e_{22}S_2 + e_{15}S_4 + \varepsilon_{11}E_2$$

$$D_3 = e_{31}S_1 + e_{31}S_2 + e_{33}S_3 + \varepsilon_{33}E_3.$$

Solutions of interest are those that describe surface wave propagation. A nonuniform plane wave solution will be assumed with propagation in one coordinate direction, attenuation in another, and independence in the third. Examination of Equations 9 and 1 indicates the optimum choice to be propagation in the x_3 direction, attenuation in the x_2 direction and no variation in the x_1 direction. Solutions of the following form are assumed for a crystal occupying the half-space $x_2 \leq 0$,

$$\begin{aligned} u_1 &= A \cdot e^{i\{k(\alpha x_2 + x_3) - \omega t\}}, \\ u_2 &= B \cdot e^{i\{k(\alpha x_2 + x_3) - \omega t\}}, \\ u_3 &= C \cdot e^{i\{k(\alpha x_2 + x_3) - \omega t\}}, \\ E_1 &= kD \cdot e^{i\{k(\alpha x_2 + x_3) - \omega t\}}, \\ E_2 &= kF \cdot e^{i\{k(\alpha x_2 + x_3) - \omega t\}}, \\ E_3 &= kG \cdot e^{i\{k(\alpha x_2 + x_3) - \omega t\}}, \quad x_2 \leq 0, \end{aligned}$$

10

where A, B, C, D, F, and G are arbitrary amplitude constants to be determined,

k is the wave number to be determined,

α is a dimensionless decay constant to be determined,

ω is the angular frequency,

t is the time.

E_1, E_2, and E_3 amplitudes include the factor of k for later convenience. Substitution of Equations 10 successively into Equations 3, 9, 1, and 6 gives the following homogeneous system of equations for surface wave propagation:

$$11 \qquad \begin{vmatrix} a_{11} & a_{12} & 0 & 0 & 0 & 0 \\ a_{21} & a_{22} & 0 & 0 & 0 & 0 \\ 0 & 0 & a_{33} & a_{34} & a_{35} & a_{46} \\ 0 & 0 & a_{43} & a_{44} & a_{45} & a_{46} \\ 0 & 0 & a_{53} & a_{54} & a_{55} & a_{56} \\ 0 & 0 & a_{63} & a_{64} & a_{65} & a_{66} \end{vmatrix} \begin{vmatrix} u_1 \\ E_1 \\ u_2 \\ u_3 \\ E_2 \\ E_3 \end{vmatrix} = 0$$

where $a_{11} = -v^2\rho + 2C_{14}\alpha + C_{55}\alpha^2 + C_{44}$,

$a_{21} = \mu_0 v^2 a_{12} = i\mu_0 v^2 (e_{15} - e_{22}\alpha)$,

$a_{22} = \mu_0 \varepsilon_{11} v^2 - \alpha^2 - 1$,

$a_{33} = -v^2\rho + C_{11}\alpha^2 - 2C_{14}\alpha + C_{44}$,

$a_{43} = a_{34} = C_{44}\alpha + C_{13}\alpha - C_{14}\alpha^2$,

$a_{53} = \mu_0 v^2 a_{35} = i\mu_0 v^2 (e_{22}\alpha + e_{15})$,

$a_{63} = \mu_0 v^2 a_{46} = i\mu_0 v^2 e_{31}\alpha$,

$a_{44} = -v^2\rho + C_{44}\alpha^2 + C_{33}$,

$a_{54} = a_{45} = ie_{15}\alpha$,

$a_{64} = \mu_0 v^2 a_{46} = i\mu_0 v^2 e_{33}$,

$a_{55} = \mu_0 \varepsilon_{11} v^2 - 1$,

$a_{65} = a_{56} = \alpha$,

$a_{66} = \mu_0 \varepsilon_{33} v^2 - \alpha^2$.

Inspection of Equations 11 indicates the existence of two uncoupled modes of propagation. One of these contains u_1 and E_1 and is described by

$$u_1 \neq 0,\ E_1 \neq 0,\ u_2 = u_3 = E_2 = E_3 = 0$$

12
$$\begin{vmatrix} a_{11} & a_{12} \\ a_{21} & a_{22} \end{vmatrix} \begin{vmatrix} u_1 \\ E_1 \end{vmatrix} = 0.$$

This solution contains nonzero components transverse to the direction of propagation and is referred to as the uncoupled transverse mode.

The second solution is described by

$$u_1 = E_1 = 0,\ u_2 \neq 0,\ u_3 \neq 0,\ E_2 \neq 0,\ E_3 \neq 0$$

13
$$\begin{vmatrix} a_{33} & a_{34} & a_{35} & a_{36} \\ a_{43} & a_{44} & a_{45} & a_{46} \\ a_{53} & a_{54} & a_{55} & a_{56} \\ a_{63} & a_{64} & a_{65} & a_{66} \end{vmatrix} \begin{vmatrix} u_2 \\ u_3 \\ E_2 \\ E_3 \end{vmatrix} = 0.$$

Here the nonzero components of displacement and electric field are coplanar, in the plane normal to the surface and parallel to the direction of propagation, such a plane is referred to as the sagittal plane and the mode is referred to as the Rayleigh mode. These two possible modes will be discussed in detail later.

Careful examination of Equations 9, 1, and 6 indicates a solution independent of x_1 is the only solution that leads to uncoupled modes. Crystals of higher symmetry have other possibilities for uncoupled modes of propagation.

As indicated previously boundary conditions must be considered to determine if either the Rayleigh or transverse mode solution is valid. Consideration of boundary conditions requires the fields outside the crystal, $x_2 > 0$, to be determined.

A. Electromagnetic Field Outside the Crystal

The assumed solutions, Equations 10, are valid for the half-space $x_2 \leq 0$ occupied by the material. The displacement components, u_i, will certainly be zero outside the material, $x_2 > 0$, but the electromagnetic fields will not. To assure matching of the fields along the surface the space and time dependence of those fields outside must be of the same form as those inside differing by amplitude constants, wave number, and decay constants only. These fields must also obey Maxwell's equations in free space,

$$14 \qquad \frac{\partial E_j}{\partial x_i \partial x_j} - \frac{\partial E_i}{\partial x_j \partial x_j} = - \varepsilon_0 \mu_0 \frac{\partial^2 E_i}{\partial t^2} ,$$

where ε_0 is the permittivity of free space, the remaining quantities are as previously defined. Assume solutions of the form

$$E_1 = kD' \cdot e^{i\{k(\beta x_2 + x_3) - \omega t\}},$$

15 $$E_2 = kF' \cdot e^{i\{k(\beta x_2 + x_3) - \omega t\}},$$

$$E_3 = kG' \cdot e^{i\{k(\beta x_2 + x_3) - \omega t\}}, \quad x_2 > 0,$$

where the decay constant β, amplitudes D', F', and G', and wave number k are to be determined. Substitution of Equations 15 into Equations 14 produces a set of homogeneous equations which govern the propagation of fields above the surface. Replacing the phase velocity, $\frac{\omega}{k}$, by v and expressing in determinant form these equations are given by Equation 16a in Table 1. This set of equations represents two uncoupled modes; one contains the E_1 component of field only, corresponding to the transverse mode, and a second contains E_2 and E_3 components representing the Rayleigh mode. For Equations 16 to have a nontrivial solution requires the coefficient determinant, Equation 16b, to be zero. The decay constant β is found from Equation 16b to be

17 $$\beta = \pm i \sqrt{(1 - \varepsilon_0 \mu_0 v^2)} .$$

Application of the boundary condition requiring fields to vanish at infinity shows the correct root to be

18 $$\beta = + i \sqrt{(1 - \varepsilon_0 \mu_0 v^2)}$$

Table 1. Equations 16a and 16b

16a

$$\begin{vmatrix} (-\beta^2 - 1 + \varepsilon_0\mu_0 v^2) & 0 & 0 \\ 0 & (1 - \varepsilon_0\mu_0 v^2) & -\beta \\ 0 & -\beta & (\beta^2 - \varepsilon_0\mu_0 v^2) \end{vmatrix} \begin{vmatrix} D' \\ F' \\ G' \end{vmatrix} = 0$$

16b

$$\begin{vmatrix} (-\beta^2 - 1 - \varepsilon_0\mu_0 v^2) & 0 & 0 \\ 0 & (1 - \varepsilon_0\mu_0 v^2) & -\beta \\ 0 & -\beta & (\beta^2 - \varepsilon_0\mu_0 v^2) \end{vmatrix} = 0$$

where the negative root is discarded as physically unrealizable. The propagation velocity of electromagnetic waves in free space is

$$19 \qquad v_0 = \frac{1}{\sqrt{\mu_0 \varepsilon_0}} .$$

Substitution of Equation 19 in Equation 18 gives

$$20 \qquad \beta = + i \sqrt{1 - (v/v_0)^2} ,$$

where $v = \frac{\omega}{k}$ is the phase velocity of acoustic waves as previously defined. The ratio of acoustic wave velocity to light wave velocity squared is of the order 10^{-10} and gives $\beta \simeq il$.

The amplitude ratio F'/G' is determined from Equation 16 to be

$$21 \qquad \frac{F'}{G'} = i \frac{1}{\sqrt{1 - \varepsilon_0 \mu_0 v^2}} = - \frac{1}{\beta} .$$

Making this substitution the electric fields outside the crystal become

$$22 \qquad \begin{aligned} E_1^+ &= kD' \cdot e^{i\{k(\beta x_2 + x_3) - \omega t\}}, \\ E_2^+ &= -k\frac{G'}{\beta} \cdot e^{i\{k(\beta x_2 + x_3) - \omega t\}}, \\ E_3^+ &= kG' \cdot e^{i\{k(\beta x_2 + x_3) - \omega t\}}, \quad x_2 > 0, \end{aligned}$$

where β is given by Equation 20.

Associated with the electric field in this region is a magnetic field found by applying Maxwell's curl equation for free space

$$\varepsilon_{ijk} \left(\frac{\partial E_k}{\partial x_j}\right) = -\mu_0 \frac{\partial H_i}{\partial t} , \tag{23}$$

to the fields of Equation 22. The magnetic fields are found to be

$$H_1^+ = - \frac{i\omega}{\mu_0 v^2} \frac{\varepsilon_0 \mu_0 v^2}{(1 - \varepsilon_0 \mu_0 v^2)^{\frac{1}{2}}} G' \cdot e^{i\{k(\beta x_2 + x_3) - \omega t\}},$$

$$H_2^+ = \frac{i\omega D'}{\mu_0 v^2} \cdot e^{i\{k(\beta x_2 + x_3) - \omega t\}}, \tag{24}$$

$$H_3^+ = - \frac{i\beta\omega D'}{\mu_0 v^2} \cdot e^{i\{k(\beta x_2 + x_3) - \omega t\}}, \quad x_2 > 0,$$

where β is given by Equation 20.

Equations 22 and 24 specify the electric and magnetic fields outside the crystal. It should be noted that for the uncoupled transverse mode $G' = 0$. Thus Equations 22 become

$$E_1^+ = kD' \cdot e^{i\{k(\beta x_2 + x_3) - \omega t\}} \tag{25}$$

and Equations 24 become

$$H_2^+ = \frac{i\omega D'}{\mu_0 v^2} \cdot e^{i\{k(\beta x_2 + x_3) - \omega t\}},$$

26

$$H_3^+ = -\frac{i\beta\omega D'}{\mu_0 v^2} \cdot e^{i\{k(\beta x_2 + x_3) - \omega t\}}.$$

For the Rayleigh mode D' = 0, Equations 22 reduce to

$$E_2^+ = -k\frac{G'}{\beta} \cdot e^{i\{k(\beta x_2 + x_3) - \omega t\}},$$

27

$$E_3^+ = kG' \cdot e^{i\{k(\beta x_2 + x_3) - \omega t\}},$$

and Equations 24 become

28 $$H_1^+ = -\frac{i\omega}{\mu_0 v^2}\left(\frac{\varepsilon_0 \mu_0 v^2}{\sqrt{1 - \varepsilon_0 \mu_0 v^2}}\right) G' \cdot e^{i\{k(\beta x_2 + x_3) - \omega t\}}.$$

Hence when boundary conditions for the transverse mode are considered the electromagnetic fields of Equations 25 and 26 are used. For the Rayleigh mode Equations 27 and 28 are used to satisfy boundary conditions. These results are summarized in Table 2.

B. Uncoupled Transverse Mode

Solution of the uncoupled transverse mode involves the simultaneous solution of Equations 12 and the boundary conditions. The expanded determinant of Equation 12 gives the secular equation for the transverse mode. If in Equations 12 the displacement u_1 and field E_1 are replaced by their respective amplitudes, A and kD, allowing the replacement

Table 2. External fields for the transverse and Rayleigh modes

	Outside Crystal $x_2 > 0$
Transverse Mode	$E_1^+ = kD' \cdot e^{i\{k(\beta x_2 + x_3) - \omega t\}}$
	$H_2^+ = \frac{i\omega D'}{\mu_0 v^2} \cdot e^{i\{k(\beta x_2 + x_3) - \omega t\}}$
	$H_3^+ = -\frac{i\beta\omega D'}{\mu_0 v^2} \cdot e^{i\{k(\beta x_2 + x_3) - \omega t\}}$
Rayleigh Mode	$E_2^+ = -k\frac{G'}{\beta} \cdot e^{i\{k(\beta x_2 + x_3) - \omega t\}}$
	$E_3^+ = kG' \cdot e^{i\{k(\beta x_2 + x_3) - \omega t\}}$
	$H_1^+ = -\frac{i\omega}{\mu_0 v^2} \frac{\varepsilon_0 \mu_0 v^2}{\beta} \cdot e^{i\{k(\beta x_2 + x_3) - \omega t\}}$

$$\beta = + i \{1 - (v/v_0)^2\}^{\frac{1}{2}}$$

of $\frac{\omega}{K}$, the phase velocity, by v the coefficient determinant is given by Equation 29 of Table 3. The secular equation is quartic in α and has real coefficients. In general there are four roots of α which must be considered in the solution. These four roots will be either real or occur in complex conjugate pairs. If the roots are real the solution does not attenuate in the x_2 direction and surface waves are not possible. For the complex conjugate pair roots the same argument holds for those two with positive imaginary parts, the two with negative imaginary parts are acceptable and do give valid surface waves. As a result of the form of the roots only two possible roots need be considered.

1. Nonpiezoelectric materials

Before developing the boundary conditions for the piezoelectric case consider the simpler nonpiezoelectric approximation to the surface wave problem. This approximation is obtained by letting the piezoelectric constants e_{15} and e_{22} go to zero in Equation 30. Note the stress components T_i reduce to those of the nonpiezoelectric case if the e_{ij}'s are set equal to zero.

For the nonpiezoelectric transverse mode to have a solution requires the determinant of Equation 30, Table 3, to be satisfied. Setting the piezoelectric constants equal to zero has the effect of uncoupling the elastic and electromagnetic waves. This uncoupling produces two independent

Table 3. Equations 29 and 30

29
$$\begin{vmatrix} (-v^2\rho + 2C_{14}\alpha + C_{66}\alpha^2 + C_{44}) & i(e_{15} - e_{22}\alpha) \\ i\mu_0 v^2 (e_{15} - e_{22}\alpha) & (\mu_0 v^2 \varepsilon_{11} - \alpha^2 - 1) \end{vmatrix} = 0$$

30
$$\begin{vmatrix} (-v^2\rho + 2C_{14}\alpha + C_{66}\alpha^2 + C_{44}) & 0 \\ 0 & (\mu_0 v^2 \varepsilon_{11} - \alpha^2 - 1) \end{vmatrix} = 0$$

modes of propagation as described by Equation 30. The first mode is a pure elastic wave whose propagation velocity and decay constants are related by

$$-v^2\rho + 2C_{14}\alpha + C_{66}\alpha^2 + C_{44} = 0. \tag{31}$$

The second mode is an electromagnetic wave whose secular equation is

$$\mu_0\varepsilon_{11}v^2 - \alpha^2 - 1 = 0. \tag{32}$$

The electromagnetic wave is of no interest since no acoustical energy is present and the wave propagates at the speed of light.

The first mode gives a possibility of a transverse mode acoustic wave. Equation 31 yields the decay constants to be

$$\alpha = -\frac{C_{14}}{C_{66}} \pm \left\{\left(\frac{C_{14}}{C_{66}}\right)^2 - \frac{C_{44}}{C_{66}} - \frac{v^2\rho}{C_{66}}\right\}^{\frac{1}{2}}. \tag{33}$$

For velocities restricted by

$$v^2 < \frac{1}{\rho}\left\{C_{44} - \left(\frac{C_{14}}{C_{66}}\right)^2\right\} \tag{34}$$

Equation 33 gives a pair of complex conjugate decay constants. The root with negative imaginary part is acceptable

and gives a surface wave providing the boundary conditions can be matched.

Boundary conditions for the nonpiezoelectric cases require a stress free surface, i.e.

$$T_2(0) = T_4(0) = T_6(0) = 0.$$

$T_2(0) = T_4(0) = 0$ is automatically satisfied by the form of the solution. $T_6(0) = 0$ requires

35 $$(2C_{14} + \alpha C_{66})u_1 = 0,$$

which for a nonzero displacement u_1 gives α as

36 $$\alpha = -\frac{2C_{14}}{C_{66}}.$$

This decay constant is real and hence does not give a surface wave. Since the boundary conditions cannot be satisfied for the transverse mode in nonpiezoelectric material no surface wave is possible. This does not, however, rule out the possible existence of the mode in piezoelectric material.

2. Piezoelectric materials

For piezoelectric material e_{15} and e_{22} are in general nonzero and the electromagnetic wave is coupled to the elastic wave as given by Equation 30. Acceptable surface wave

solutions are given by two of the possible four roots of α. Due to the algebraic complexity of determining these values of α explicitly from Equation 29 the two distinct roots will be assumed to exist and a linear superposition of solutions will be made for these two roots. The assumed solutions then become

$$u_1 = \sum_j A_j \cdot e^{i\{k(\alpha_j x_2 + x_3) - \omega t\}}, \tag{37a}$$

$$E_1 = \sum_j kD_j \cdot e^{i\{k(\alpha_j x_2 + x_3) - \omega t\}}, \quad j = 1,2 \text{ and } x_2 \leq 0. \tag{37b}$$

Expressing D_j in terms of an amplitude ratio allows Equation 37b to be expressed as

$$E_1 = \sum_j km_j A_m \cdot e^{i\{k(\alpha_j x_2 + x_3) - \omega t\}}, \tag{38}$$

where m_j is determined from Equation 30 to be

$$m_j = \frac{D_j}{A_j} = - \frac{i\mu_0 v^2 (e_{15} - e_{22}\alpha_j)}{\mu_0 \epsilon_{11} v^2 - \alpha_j^2 - 1}. \tag{39}$$

Boundary conditions require, as in the nonpiezoelectric approximation, a stress free surface, and in addition continuity of appropriate magnetic fields across the surface. A stress free surface requires

$$T_2(0) = T_4(0) = T_6(0) = 0, \tag{40}$$

where $T_2(0) = T_4(0) = 0$ is automatically satisfied by the form of the solution. Substituting the assumed solutions, Equations 37a and 38, into Equations 9 finds $T_6(0) = 0$ requires

41 $$\sum_j (2C_{14} + \alpha_j C_{66} + e_{22} m_j) A_j = 0, \quad j = 1,2.$$

Continuous tangential magnetic field intensity components across the interface require

42a $$H_3^-(0) = H_3^+(0).$$

Continuous normal components of the flux density require

42b $$\mu_0 H_3^-(0) = \mu_0 H_3^+(0).$$

$H_2^+(0)$ and $H_3^+(0)$ are obtained from Table 2 while $H_2^-(0)$ and $H_3^-(0)$ are found by substituting Equation 38 into Maxwell's curl equation, Equation 23, obtaining

43a $$H_2^- = \sum_j \frac{i\omega}{\mu_0 v^2} m_j A_j \cdot e^{i\{k(\alpha_j x_2 + x_3) - \omega t\}},$$

43b $$H_3^- = \sum_j \frac{i\omega}{\mu_0 v^2} \alpha_j m_j A_j \cdot e^{i\{k(\alpha_j x_2 + x_3) - \omega t\}}, \quad j = 1,2.$$

Making these substitutions Equation 42a gives

44a $$D' = \sum_j m_j A_j, \quad @y = 0, \quad j = 1,2,$$

and Equation 42b gives

44b $$\beta D' = \sum_j \alpha_j m_j A_j, \quad @y = 0, \quad j = 1,2.$$

Combining Equations 44a and 44b gives the electromagnetic field boundary condition as

45 $$\sum_j (\alpha_j - \beta) m_j A_j = 0, \quad j = 1,2.$$

Boundary conditions for the transverse mode can be summarized by combining Equations 41 and 45 to obtain the homogeneous set of Equation 46 of Table 4. A nontrivial solution of Equation 46 requires the coefficient determinant to be zero, Equation 47 of Table 4.

To determine the appropriate values of α_1, α_2, and v Equation 48 and the secular equation, the expanded determinant of Equation 30, are solved simultaneously. The values of α_1 and α_2 which simultaneously satisfy these equations and are complex with negative imaginary parts are valid solutions of the transverse mode.

In formulating the boundary conditions distinct roots were assumed. If a degenerate root is present the boundary conditions must be reformulated for an assumed solution containing one distinct root. This is quite easily done

Table 4. Equations 46 and 47

46
$$\begin{vmatrix} (C_{14} + \alpha_1 C_{66} + e_{22} m_1) & (C_{14} + \alpha_2 C_{66} + e_{22} m_2) \\ (\alpha_1 - \beta) m_1 & (\alpha_2 - \beta) m_2 \end{vmatrix} \begin{vmatrix} A_1 \\ A_2 \end{vmatrix} = 0$$

47
$$\begin{vmatrix} (C_{14} + \alpha_1 C_{66} + e_{22} m_1) & (C_{14} + \alpha_2 C_{66} + e_{22} m_2) \\ (\alpha_1 - \beta) m_1 & (\alpha_2 - \beta) m_2 \end{vmatrix} = 0$$

and can be shown to result in one column of Equation 47 equal to zero. This would require $\alpha = \beta$. Since β has been determined to be positive and imaginary, Equation 20, degenerate roots do not give valid surface wave solutions.

Only two possibilities remain for α_1 and α_2. If they are negative, imaginary, and distinct a transverse mode exists which exponentially attenuates away from the surface, $x_2 = 0$, and propagates along it. This mode will be referred to as the pure transverse mode. The other possibility is for α_1 and α_2 to be distinct complex numbers with negative imaginary parts and nonzero real parts. This gives a valid surface wave which propagates at an angle to the surface. Such a mode will be referred to as a generalized transverse mode.

The pure transverse mode in trigonal crystals for the propagation direction and orientation considered here is discussed for the general case in the Appendix. Algebraic manipulations of the secular equation demonstrate that the pure mode cannot exist.

Unfortunately the generalized transverse mode is not as easily investigated. To determine the possible existence of this mode would require a numerical solution. These results would be applicable to $LiNbO_3$ only, however, and no general results for trigonal crystals would be obtained. Since this mode would not be excited by the interdigital transducers it will not be considered further.

C. Rayleigh Mode

Solution of the Rayleigh mode consists of satisfying the secular equation found from Equations 13 and the boundary conditions associated with this mode. The secular equation for the Rayleigh mode with the phase velocity $\frac{\omega}{k}$ replaced by v is the expanded coefficient determinant of Equation 48, Table 5. Expansion of the coefficient determinant yields a sextic equation with real coefficients. The six roots of this equation are either real or occur in complex conjugate pairs. As discussed for the transverse mode only certain roots allow surface waves to exist, namely the complex roots with negative imaginary parts. Therefore of the total six roots only three pertain to surface waves. These three roots which pertain to surface wave propagation may occur in different forms giving different types of solutions. The different possibilities are discussed below.

Case 1. The three roots are pure imaginary numbers, i.e. zero real parts, all of which are less than zero. These roots give a solution which propagates in the X_3-direction and is attenuated in the X_2-direction. A mode of this type was originally discussed by Rayleigh (9) and has been referred to by Synge (12) as a pure Rayleigh mode.

Case 2. The three roots have nonzero real parts and negative imaginary parts. The real part of these roots contributes a phase component to the solution. Waves for

Table 5. Equations 48 and 49

48

$$\begin{vmatrix} (-v^2\rho + C_{11}\alpha^2 - 2C_{14}\alpha + C_{44}) & (C_{13}\alpha - C_{14}\alpha^2 + C_{44}\alpha) & i(e_{22}\alpha + e_{15}) & (ie_{31}\alpha) \\ (-C_{14}\alpha^2 + C_{44}\alpha + C_{13}\alpha) & (-v^2\rho + C_{44}\alpha^2 + C_{33}) & (ie_{15}\alpha) & (ie_{33}) \\ i\mu_0 v^2(e_{22}\alpha + e_{15}) & (i\mu_0 v^2 e_{15}\alpha) & (\mu_0\varepsilon_{11}v^2 - 1) & (\alpha) \\ (i\mu_0 v^2 e_{31}\alpha) & (i\mu_0 v^2 e_{33}) & (\alpha) & (\mu_0\varepsilon_{33}v^2 - \alpha^2) \end{vmatrix} \begin{vmatrix} B \\ C \\ F \\ G \end{vmatrix} = 0$$

49

$$\begin{vmatrix} (-v^2\rho + C_{11}\alpha^2 - 2C_{14}\alpha + C_{44}) & (C_{13}\alpha - C_{14}\alpha^2 + C_{44}\alpha) & 0 & 0 \\ (-C_{14}\alpha^2 + C_{44}\alpha + C_{13}\alpha) & (-v^2\rho + C_{44}\alpha^2 + C_{33}) & 0 & 0 \\ 0 & 0 & (\mu_0\varepsilon_{11}v^2 - 1) & (\alpha) \\ 0 & 0 & (\alpha) & (\mu_0\varepsilon_{33}v^2 - \alpha^2) \end{vmatrix} \begin{vmatrix} B \\ C \\ F \\ G \end{vmatrix} = 0$$

these roots are attenuated in the X_2-direction but also contain a phase component in that direction. Synge (12) referred to waves of this type as generalized Rayleigh waves.

Case 3. A combination of Case 1 and Case 2 is also possible. A solution of this type would produce a superposition of the two modes.

1. Nonpiezoelectric materials

Before proceeding with the general piezoelectric case a nonpiezoelectric approximation will again be made to investigate the possible existence of this mode in nonpiezoelectric elastic media. Examination of Equation 48 indicates that setting $e_{22} = e_{15} = e_{33} = e_{31} = 0$ for the approximation produces two uncoupled modes out of the piezoelectric Rayleigh mode. One of these modes, the lower right hand two by two in Equation 49, has the form identical to that of the electromagnetic field outside the crystal, Equation 16, and is therefore a pure electromagnetic wave with no acoustical part. The upper left hand two by two is the pure elastic mode with no electromagnetic part. To investigate the possibility of an elastic wave for this mode consider the secular equation to be given by the expanded coefficient determinant of

$$50 \quad \begin{vmatrix} (-v^2\rho + C_{11}\alpha^2 - 2C_{14}\alpha + C_{44}) & (C_{13}\alpha - C_{14}\alpha^2 + C_{44}\alpha) \\ (-C_{14}\alpha^2 + C_{44}\alpha + C_{13}\alpha) & (-v^2\rho + C_{44}\alpha^2 + C_{33}) \end{vmatrix} \begin{vmatrix} B \\ C \end{vmatrix} = 0$$

The expanded form of Equation 50 is a quartic equation with real coefficients. Of the four possible roots for α only two satisfy the boundary condition that fields and displacements go to zero at infinity. The solutions for the non-piezoelectric approximation therefore take the following form

$$51a \qquad u_2 = \sum_j B_j \cdot e^{i\{k(\alpha_j x_2 + x_3) - \omega t\}},$$

$$51b \qquad u_3 = \sum_j C_j \cdot e^{i\{k(\alpha_j x_2 + x_3) - \omega t\}}, \quad j = 1,2, \quad x_2 \leq 0$$

where the summation on j corresponds to the two roots α_1 and α_2. Defining the amplitude ratio $n_j = \frac{C_j}{B_j}$, the u_3 displacement can be rewritten as

$$52 \qquad u_3 = \sum_j n_j B_j \cdot e^{i\{k(\alpha_j x_2 + x_3) - \omega t\}},$$

where n_j is found from Equation 50 to be

$$53 \qquad n_j = \frac{-v^2\rho + C_{11}\alpha_j^2 - 2C_{14}\alpha_j + C_{44}}{C_{13}\alpha_j - C_{14}\alpha_j^2 + C_{44}\alpha_j}, \quad j = 1,2.$$

Boundary conditions for this mode again require normal components of stress to vanish at the surface, i.e.

$$54 \qquad T_2(0) = T_4(0) = T_6(0) = 0.$$

$T_6(0)$ is automatically satisfied by the form of the assumed solution and $T_2(0)$ and $T_4(0)$ are found by substituting Equation 51 in Equations 9 to get

$$55a \qquad T_2(0) = \sum_j \{(\alpha_j C_{11} - C_{14}) + (C_{13} - \alpha_j C_{14}) n_j\} B_j = 0$$

and

$$55b \qquad T_4(0) = \sum_j \{(C_{44} - \alpha_j C_{14}) + C_{44} \alpha_j n_j\} B_j = 0, \quad j = 1,2.$$

Equations 55 written in matrix form are in Table 6, Equation 56. This set of homogeneous equations requires the coefficient determinant to be zero for a nontrivial solution, as given by Equation 57 of Table 6.

Formally Equations 50 and 57 can be solved simultaneously to find the decay constants, α, and propagation velocity, v. In practice this is extremely tedious due to the algebraic complexity of the equations. To determine α and v a numerical technique will be employed where a value of v is chosen and substituted in Equation 50 and the corresponding values of α determined. These values, α_1, α_2, and v, are then substituted into Equation 57 to see if the boundary conditions are satisfied. If Equation 57 is not satisfied a new value of v is chosen and the process repeated until both Equation 50 and Equation 57 are satisfied simultaneously. Assuming this process gives the correct

Table 6. Equations 56 and 57

$$56 \quad \begin{vmatrix} \{(\alpha_1 C_{11} - C_{14}) + (C_{13} - \alpha_1 C_{14})n_1\} & \{(\alpha_2 C_{11} - C_{14}) + (C_{13} - \alpha_2 C_{14})n_2\} \\ \{(C_{44} - \alpha_1 C_{14}) + C_{44}\alpha_1 n_1\} & \{(C_{44} - \alpha_2 C_{14}) + C_{44}\alpha_2 n_2\} \end{vmatrix} \begin{vmatrix} B_1 \\ B_2 \end{vmatrix} = 0$$

$$57 \quad \begin{vmatrix} \{(\alpha_1 C_{11} - C_{14}) + (C_{13} - \alpha_1 C_{14})n_1\} & \{(\alpha_2 C_{11} - C_{14}) + (C_{13} - \alpha_2 C_{14})n_2\} \\ \{(C_{44} - \alpha_1 C_{14}) + C_{44}\alpha_1 n_1\} & \{(C_{44} - \alpha_2 C_{14}) + C_{44}\alpha_2 n_2\} \end{vmatrix} = 0$$

decay constants and propagation velocity the final form of the solutions can be formulated.

A second amplitude ratio is defined from Equation 57 as

$$58 \qquad m_{21} = \frac{B_2}{B_1} = \frac{(\alpha_1 C_{11} - C_{14}) + (C_{13} - \alpha_1 C_{14})n_1}{(\alpha_2 C_{11} - C_{14}) + (C_{13} - \alpha_2 C_{14})n_2} .$$

Utilizing Equation 58 the final form of the displacement terms for nonpiezoelectric approximation to the Rayleigh mode can be written as

$$59 \qquad \begin{aligned} u_2 &= B_1\{e^{i\alpha_1 kx_2} + m_{21}e^{i\alpha_2 kx_2}\}e^{i(kx_3 - \omega t)} \\ u_3 &= n_1 B_1\{e^{i\alpha_1 kx_2} + n_{21}e^{i\alpha_2 kx_2}\}e^{i(kx_3 - \omega t)} \end{aligned}$$

where

$$60 \qquad n_{21} = \left(\frac{n_2}{n_1}\right) m_{21}.$$

a. Numerical results for nonpiezoelectric approximation

Warner, Onoe, and Coquin (16) have measured the elastic, piezoelectric, and dielectric constants for $LiNbO_2$. These results are tabulated in Table 7. Piezoelectric constants are included since they will be needed later. The density was measured by Nassau, Levinstein and Loiacono (8).

Table 7. Physical properties of $LiNbO_3$

Elastic constants ($x10^{11} N/m^2$)	Piezoelectric constants (c/m^2)	Dielectric constants	Density (kg/m^3)
$C_{11} = 2.03$	$e_{15} = 3.7$	$\varepsilon_{11}/\varepsilon_0 = 44$	4.64×10^3
$C_{12} = 0.53$	$e_{22} = 2.5$	$\varepsilon_{33}/\varepsilon_0 = 29$	
$C_{13} = 0.75$	$e_{31} = 0.2$		
$C_{14} = 0.09$	$e_{33} = 1.3$		
$C_{33} = 2.45$			
$C_{44} = 0.60$			
$C_{66} = 0.75$			

The elastic and dielectric constants are measured at constant entropy and constant strain respectively as specified in the problem formulation. ε_0 is the permittivity of free space. and in rationalized MKS units is $(1/36\pi) \times 10^{-9}$.

These constants are substituted into Equations 50 and 57. The resulting set of equations is then solved numerically for v, α_1, and α_2 as described in the previous section. When these equations are simultaneously satisfied a solution has been found which satisfied both the secular equation and boundary conditions. Providing the values of α determined by this procedure give valid surface waves the solution is complete. Results of the described method are given in

Table 8.

Table 8. Propagation velocity and dimensionless decay constants for the nonpiezoelectric approximation in $LiNbO_3$

v (m/sec)	α_1	α_2
3.3924×10^3	0.08734 - i0.2297	-0.1431 - i1.3073

These values are then substituted into Equation 53 to obtain the amplitude ratios, n_1 and n_2, and Equation 58 and 60 to obtain m_{21} and n_{21} respectively. These amplitude ratios are found in Table 9.

Table 9. Dimensionless amplitude ratios for the nonpiezoelectric approximation

$n_1 = -0.0666 + i0.1614$	$m_{21} = -0.2947 - i0.1726$
$n_2 = 0.5105 + i1.8672$	$n_{21} = -3.7549 + i0.4854$

Values given in Tables 8 and 9 are substituted into Equations 59 to obtain the final form of the displacements u_2 and u_3. Omitting the $e^{i(kx_3 - \omega t)}$ dependence gives

$$u_2 = B_1\{e^{ik(0.08734 - i0.2297)x_2} - (0.2947 + i0.1726)e^{ik(-0.1431 - i1.3073)x_2}\}, \tag{61a}$$

$$u_3 = B_1(-0.0666 + i0.1614)\{e^{ik(0.08734 - i0.2297)x_2} - (3.7549 - i0.4854)e^{ik(-0.1431 - i1.3073)x_2}\}, \tag{61b}$$

where B_1 is an arbitrary amplitude constant.

Table 8 indicates the roots are of the form discussed in Case 2 of this section. The solutions represent the generalized Rayleigh mode of propagation. To remove the arbitrary constant, B_1, from Equations 61 the solutions are normalized with respect to $u_2(0)$, the displacement of u_2 at the surface. The depth into the crystal is also normalized so that it is measured in wavelengths. Making the above modifications Equations 61 become

$$\frac{u_2}{u_2(0)} = \frac{e^{i2\pi\alpha_1 d} + m_{21}e^{i2\pi\alpha_2 d}}{1 + m_{21}}, \tag{62a}$$

$$\frac{u_3}{u_2(0)} = \frac{n_1(e^{i2\pi\alpha_1 d} + n_{21}e^{i2\pi\alpha_2 d})}{1 + m_{21}}, \tag{62b}$$

where d is depth in wavelengths and the other symbols are as previously defined.

Evaluation of Equations 62 yields a complex number. To plot displacement amplitude versus depth the data obtained from Equations 62 are converted to polar form. The plot of

Figure 1 shows the amplitude variation with depth. The normalized displacements were plotted by using the magnitude of the polar form. Phase information was suppressed except for the $u_3/u_2(0)$ plot where the displacement goes negative at about 0.25λ. This behavior was graphed as shown to indicate that the displacement, $u_3/u_2(0)$, does pass through zero.

The phase change of the displacements is shown in Figure 2. This graph indicates a transient phenomenon for a fraction of a wavelength. The two displacements then settle down to a constant phase difference, approximately 112^{o}, and a linear phase variation. The initial disturbance is possibly caused by the boundary condition requirements of a free surface.

2. Piezoelectric materials

Solution of the Rayleigh mode in piezoelectric crystals is similar to the nonpiezoelectric approximation. However, due to the coupling of the electromagnetic field and the elastic wave by the piezoelectric constants the secular equation, found by expanding Equation 48, becomes a sextic with real coefficients as noted earlier. The three acceptable roots are used to obtain the assumed solution as a linear combination

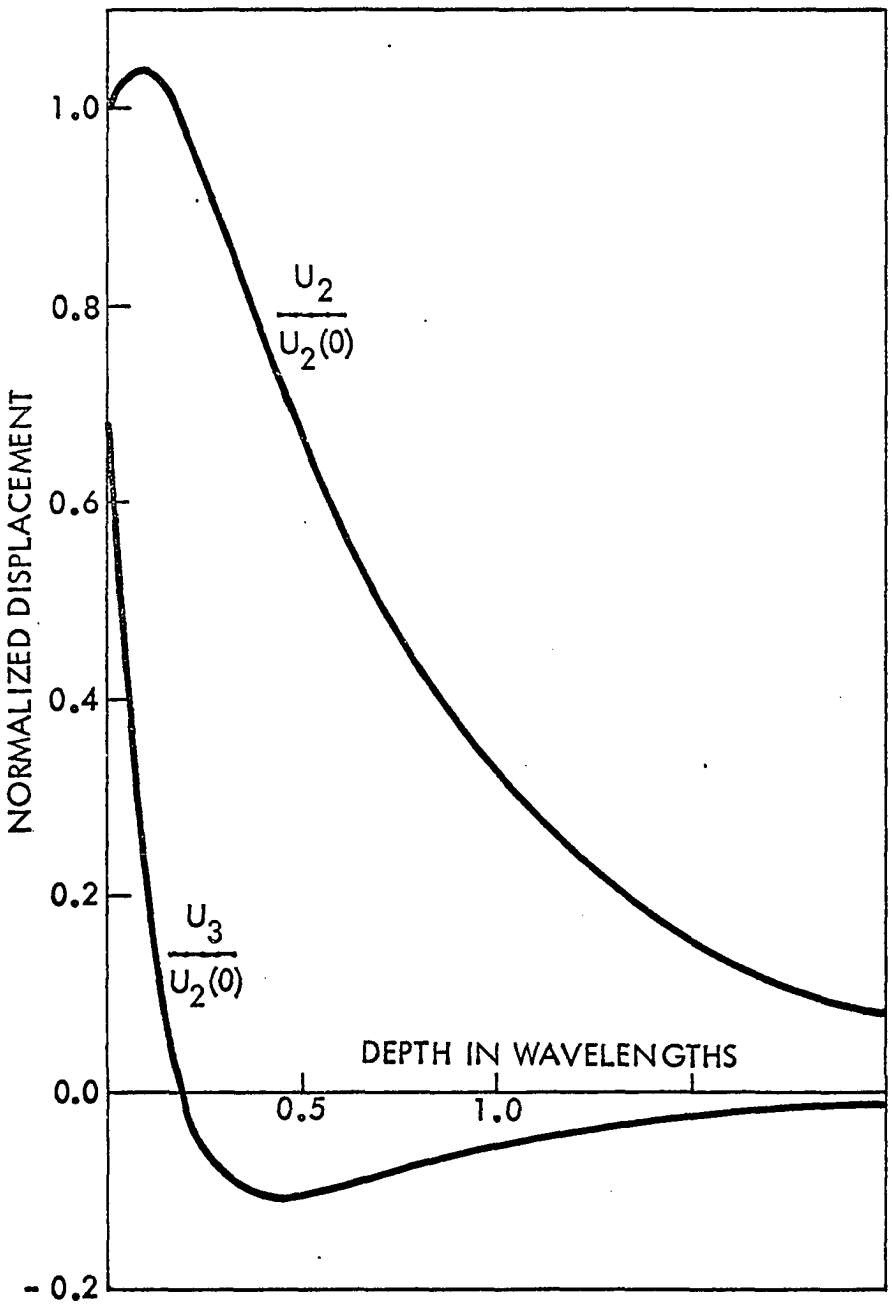

Figure 1. Normalized particle displacement versus depth for nonpiezoelectric surface wave propagation on $LiNbO_3$

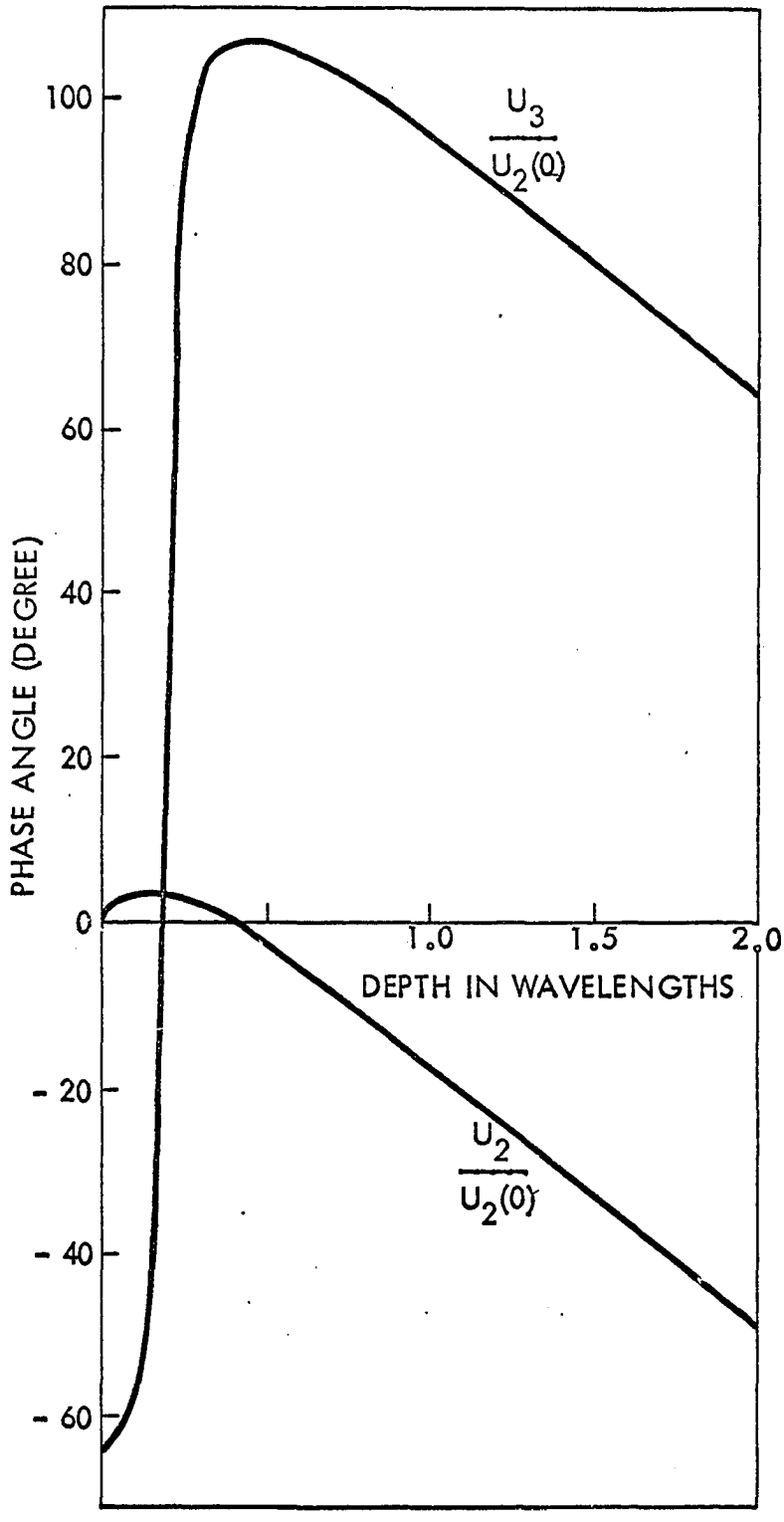

Figure 2. Phase relation of the displacement components for nonpiezoelectric surface wave propagation on $LiNbO_3$

$$u_2 = \sum_j B_j \cdot e^{i\{k(\alpha_j x_2 + x_3) - \omega t\}},$$

$$u_3 = \sum_j C_j \cdot e^{i\{k(\alpha_j x_2 + x_3) - \omega t\}},$$

63

$$E_2 = \sum_j kF_j \cdot e^{i\{k(\alpha_j x_2 + x_3) - \omega t\}},$$

$$E_3 = \sum_j kG_j e \cdot i\{k(\alpha_j x_2 + x_3) - \omega t\}, \quad j = 1,2,3, \quad x_2 \leq 0.$$

Amplitude ratios are defined as

$$n_j = \frac{C_j}{B_j},$$

64

$$o_j = \frac{F_j}{B_j},$$

$$p_j = \frac{G_j}{B_j}, \quad j = 1,2,3,$$

where n_j, o_j, and p_j are determined from Equation 48. To determine these ratios recall that the complete solution of a homogeneous system is given by

65 $$x_i = c(-1)^{i+1}|M_i|, \quad i = 1,2,3,\cdots,n$$

where x_i is the amplitude of interest,

c is an arbitrary scalar constant,

$|M_i|$ is the determinant of the matrix M_i, obtained from M, a submatrix of the coefficient matrix, by deleting the i^{th} column.

Applying the result of Equation 65 the amplitude ratios

are found in Table 10. These amplitude ratios can be used to express the solutions in terms of the amplitude constants B_j as

$$u_2 = \sum_j B_j \cdot e^{i\{k(\alpha_j x_2 + x_3) - \omega t\}},$$

$$u_3 = \sum_j n_j B_j \cdot e^{i\{k(\alpha_j x_2 + x_3) - \omega t\}},$$

67

$$E_2 = \sum_j ko_j B_j \cdot e^{i\{k(\alpha_j x_2 + x_3) - \omega t\}},$$

$$E_3 = \sum_j kp_j B_j \cdot e^{i\{k(\alpha_j x_2 + x_3) - \omega t\}}, \quad j = 1,2,3, \quad x_2 \leq 0.$$

Equations 67 are used to determine the requirements of the boundary conditions. A stress free surface is again required as discussed in the nonpiezoelectric approximation case. This requires $T_2(0) = 0$ and $T_4(0) = 0$, or

$$T_2(0) = \sum_j \{(\alpha_j C_{11} - C_{14}) + C_{13} - \alpha_j C_{14})n_j - ie_{22}o_j$$

68a

$$-ie_{31}p_j\}B_j = 0,$$

$$T_4(0) = \sum_j \{(C_{44} - \alpha_j C_{14}) + C_{44}\alpha_j n_j - ie_{15}o_j\}B_j = 0,$$

68b

$$j = 1,2,3.$$

In addition to Equations 68 the tangential electric field, E_3, must be continuous across the boundary; the normal electric flux density must also be continuous at $x_2 = 0$. The

Table 10. Equations 66

$$66a \quad n_j = \frac{C_j}{B_j} = -\frac{1}{\Delta_j} \begin{vmatrix} (-v^2\rho + C_{11}\alpha_j^2 - 2C_{14}\alpha_j + C_{44}) & i(e_{22}\alpha_j + e_{15}) & (ie_{31}\alpha_j) \\ (-C_{14}\alpha_j^2 + C_{44}\alpha_j + C_{14}\alpha_j) & (ie_{15}\alpha_j) & (ie_{33}) \\ i\mu_0 v^2 (e_{22}\alpha_j + e_{15}) & (\mu_o \varepsilon_{11} v^2 - 1) & (\alpha_j) \end{vmatrix}$$

$$66b \quad o_j = \frac{F_j}{B_j} = \frac{1}{\Delta_j} \begin{vmatrix} (-v^2\rho + C_{11}\alpha_j^2 - 2C_{14}\alpha_j + C_{44}) & (C_{13}\alpha_j - C_{14}\alpha_j^2) & (ie_{31}\alpha_j) \\ (-C_{14}\alpha_j^2 + C_{44}\alpha_j + C_{13}\alpha_j) & (-v^2\rho + C_{44}\alpha_j^2 + C_{33})(ie_{33}) \\ i\mu_0 v^2 (e_{22}\alpha_j + e_{15}) & (ie_{15}\alpha_j) & (\alpha_j) \end{vmatrix}$$

Table 10 (Continued)

66c

$$p_j = \frac{C_j}{B_j} = -\frac{1}{\Delta_j}\begin{vmatrix} (-v^2\rho + C_{11}\alpha_j^2 - 2C_{14}\alpha_j + C_{44}) & (C_{13}\alpha_j - C_{14}\alpha_j^2 + C_{44}\alpha_j) & i(e_{22}\alpha_j + e_{15}) \\ (-C_{14}\alpha_j^2 + C_{44}\alpha_j + C_{13}\alpha_j) & (-v^2\rho + C_{44}\alpha_j^2 + C_{33}) & (ie_{15}\alpha_j) \\ i\mu_0 v^2(e_{22}\alpha_j + e_{15}) & (ie_{15}\alpha_j) & (\mu_0\varepsilon_{11}v^2 - 1) \end{vmatrix}$$

66d

$$\Delta_j = \begin{vmatrix} (C_{13}\alpha_j - C_{14}\alpha_j^2) & i(e_{22}\alpha_j + e_{15}) & (ie_{31}\alpha_j) \\ (-v^2\rho + C_{44}\alpha_j^2 + C_{33}) & (ie_{15}\alpha_j) & (ie_{33}) \\ (ie_{15}\alpha_j) & (\mu_0\varepsilon_{11}v^2 - 1) & (\alpha_j) \end{vmatrix}$$

tangential electric field requires

$$E_3^+(0) = E_3^-(0). \tag{69}$$

Substitution of $E_3^+(0)$ from Equation 27 and $E_3^-(0)$ from Equation 67 gives

$$G' = \sum_j p_j B_j, \quad j = 1,2,3. \tag{70}$$

Normal component of electric flux density requires

$$D_2^-(0-) = \varepsilon_0 E_2^+(0), \tag{71}$$

substitution from Equation 27 for $E_2^+(0)$ and Equations 67 into Equations 9 for $D_2^-(0)$ gives

$$\sum_j \{i(e_{22}\alpha_j + e_{15}) + ie_{15}\alpha_j n_j + \varepsilon_{22} o_j\} B_j + \varepsilon_0 \frac{G'}{\beta} = 0. \tag{72}$$

Substitution of Equation 70 for G' gives the final form of the electromagnetic boundary conditions from Equation 72 to be

$$\sum_j \{i(e_{22}\alpha_j + e_{15}) + ie_{15}\alpha_j n_j + \varepsilon_{22} o_j - \left(\frac{i\varepsilon_0}{\sqrt{1 - \varepsilon_0 \mu_0 v^2}}\right) p_j\} B_j = 0, \tag{73}$$

$$j = 1,2,3.$$

Boundary conditions given by Equations 68 and 73 can be summarized by a homogeneous system

$$74 \qquad \begin{vmatrix} b_{11} & b_{12} & b_{13} \\ b_{21} & b_{22} & b_{23} \\ b_{31} & b_{32} & b_{33} \end{vmatrix} \begin{vmatrix} B_1 \\ B_2 \\ B_3 \end{vmatrix} = 0.$$

This system requires the coefficient determinant to be zero for a nontrivial solution,

$$75 \qquad \begin{vmatrix} b_{11} & b_{12} & b_{13} \\ b_{21} & b_{22} & b_{23} \\ b_{31} & b_{32} & b_{33} \end{vmatrix} = 0,$$

where $b_{1j} = (\alpha_j C_{11} - C_{14}) + (C_{13} - \alpha_j C_{14})n_j - ie_{22}o_j - ie_{31}p_j$

$$b_{2j} = (C_{44} - \alpha_j C_{14}) + C_{44}\alpha_j n_j - ie_{15}o_j$$

$$b_{3j} = i(e_{22}\alpha_j + e_{15}) + ie_{15}\alpha_j n_j + \varepsilon_{22}o_j - \left(\frac{i\varepsilon_o}{\sqrt{1 - \varepsilon_0\mu_0 v^2}}\right)p_j$$

$$j = 1,2,3.$$

For reasons discussed in the approximation section a numerical technique must be employed to determine the values of α_1, α_2, and v that simultaneously satisfy the coefficient determinants of Equation 48 and Equation 74 equal to zero.

The results of this numerical technique are discussed in the next section. The final form of the solutions can be obtained as follows:

$$u_2 = B_1\{e^{i\alpha_1 kx_2} + m_{21}e^{i\alpha_2 kx_2} + m_{31}e^{i\alpha_3 kx_2}\}e^{i\{kx_3 - \omega t\}},$$

$$u_3 = N_1B_1\{e^{i\alpha_1 kx_2} + n_{21}e^{i\alpha_2 kx_2} + n_{31}e^{i\alpha_3 kx_2}\}e^{i\{kx_3 - \omega t\}},$$

76 $$E_2 = ko_1B_1\{e^{i\alpha_1 kx_2} + o_{21}e^{i\alpha_2 kx_2} + o_{31}e^{i\alpha_3 kx_2}\}e^{i\{kx_3 - \omega t\}},$$

$$E_3 = kp_1B_1\{e^{i\alpha_1 kx_2} + p_{21}e^{i\alpha_2 kx_2} + p_{31}e^{i\alpha_3 kx_2}\}e^{i\{kx_3 - \omega t\}},$$

$$E_1 = u_1 = 0, \quad x_2 \leq 0.$$

The amplitude ratios b_{j1}, n_{j1}, o_{j1}, and p_{j1} are determined using the technique of Equation 65 and the determinant of Equation 75 to be

77 $$m_{21} = \frac{B_2}{B_1} = -\frac{1}{\Delta}(b_{11}b_{23} - b_{21}b_{13}),$$
$$m_{31} = \frac{B_3}{B_1} = \frac{1}{\Delta}(b_{11}b_{22} - b_{12}b_{21}),$$

where $\Delta = (b_{11}b_{23} - b_{22}b_{13})$, and the others are related by

78 $$n_{j1} = (\frac{n_j}{n_1})m_{j1},$$
$$o_{j1} = (\frac{o_j}{o_1})m_{j1},$$
$$p_{j1} = (\frac{p_j}{p_1})m_{j1}, \quad j = 2,3.$$

a. Numerical results for piezoelectric material

A technique similar to that used for the approximation is now used to evaluate the numerical values of the amplitude ratios, decay constants, and propagation velocity just described. The numerical solution for this case involves finding the roots of the secular equation, Equation 48, for various values of propagation velocity. These sets of values, a propagation velocity and three decay constants, are then substituted into the boundary condition determinant, Equation 75, to find which set simultaneously satisfies both the secular equation and the boundary conditions. The necessary values of elastic constants, piezoelectric constants, and permittivities are found in Table 7.

Table 11 gives the values of decay constants and propagation velocity found by the numerical technique.

Table 11. Propagation velocity and dimensionless decay constants for the piezoelectric solution in $LiNbO_3$

$v = 3.5105 \times 10^3$
$\alpha_1 = 0.06462 - i0.1217$
$\alpha_2 = 0.3804 - i1.0379$
$\alpha_3 = -0.3960 - i0.7738$

The form of the decay constants, α_1, α_2, and α_3 indicate that the generalized Rayleigh mode is found as the solution. These values are then substituted into Equations 66, 77 and 78 to determine the amplitude ratios m_{21}, m_{31}, n_1, n_{21}, n_{31}, o_1, o_{21}, o_{31}, p_1, p_{21}, and p_{31} needed to determine the solutions given by Equations 76. The amplitude ratios are tabulated in Table 12. The dimensions of p_1 and o_1 are volts per meter, while the rest are dimensionless.

Table 12. Dimensionless amplitude ratios for the piezoelectric solution

$m_{21} = -0.02637 + i0.3719$	$n_1 = -0.05180 + i0.09719$
$m_{31} = 0.02740 - i0.5141$	$n_{21} = -1.9258 + i5.0940$
	$n_{31} = -4.1163 - i1.4533$
$o_1 = (-0.1826 + i0.1402) \times 10^9$	$p_1 = (-1.5202 - i0.6931) \times 10^9$
$o_{21} = (-0.3243 - i0.2219) \times 10^2$	$p_{21} = -3.6274 - i3.2912$
$o_{31} = (0.2723 + i0.1945) \times 10^2$	$p_{31} = -0.05632 + i5.3042$

Tables 11 and 12 contain the information needed to write the final form of the solution for piezoelectric surface wave propagation in $LiNbO_3$. Omitting the $e^{i(kx_3 - \omega t)}$ dependence the solutions are

$$u_2 = B_1\{e^{ik(0.06462 - i0.1217)x_2}$$

$$+ (-0.02637 + i0.3719)e^{ik(0.3804 - i1.0379)x_2}$$

$$+ (0.02740 - i0.5141)e^{ik(-0.3960 - i0.7738)x_2}\},$$

$$u_3 = B_1(-0.05180 + i0.09719)\{e^{ik(0.06462 - i0.1217)x_2}$$

$$+ (-1.9258 + i5.0940)e^{ik(0.3804 - i1.0379)x_2}$$

79

$$+ (-4.1163 - i1.4533)e^{ik(-0.3960 - i0.7738)x_2}\},$$

$$E_2 = kB_1(-0.1826 + i0.1402) \times 10^9\{e^{ik(0.06462 - i0.1217)x_2}$$

$$+ (-0.3243 - i0.2219) \times 10^2 e^{ik(0.3804 - i1.0379)x_2}$$

$$+ (0.2723 + i0.1945) \times 10^2 e^{ik(-0.3960 - i0.7738)x_2}\},$$

$$E_3 = kB_1(-1.5202 - i0.6931) \times 10^9\{e^{ik(0.06462 - i0.1217)x_2}$$

$$+ (-3.6274 - i3.2912)e^{ik(0.3804 - i1.0379)x_2}$$

$$+ (-0.05632 + i5.3042)e^{ik(-0.3960 - i0.7738)x_2}\},$$

$$x_2 \leq 0.$$

Equations 79 describe the behavior of surface wave propagation in $LiNbO_3$ in terms of an arbitrary constant, B_1. B_1 is removed by a normalization process similar to that used for the approximation method. Depth variation into the

crystal is also normalized so that it is measured in wavelengths; resulting equations are

$$\frac{u_2}{u_2(0)} = \frac{e^{i2\pi\alpha_1 d} + m_{21}e^{i2\pi\alpha_2 d} + m_{31}e^{i2\pi\alpha_3 d}}{1 + m_{21} + m_{31}}$$

$$\frac{u_3}{u_2(0)} = \frac{n_1(e^{i2\pi\alpha_1 d} + n_{21}e^{i2\pi\alpha_2 d} + n_{31}e^{i2\pi\alpha_3 d})}{1 + m_{21} + m_{31}}$$

80

$$\frac{E_2}{E_2(0)} = \frac{e^{i2\pi\alpha_1 d} + o_{21}e^{i2\pi\alpha_2 d} + o_{31}e^{i2\pi\alpha_3 d}}{1 + o_{21} + o_{31}}$$

$$\frac{E_3}{E_2(0)} = \frac{p_1(e^{i2\pi\alpha_1 d} + p_{21}e^{i2\pi\alpha_2 d} + p_{31}e^{i2\pi\alpha_3 d})}{o_1(1 + o_{21} + o_{31})}$$

$$x_2 \leq 0.$$

The amplitude ratios are those given in Table 12 and d is depth of penetration measured in wavelengths. $u_2(0)$ and $E_2(0)$ are the values of the displacement and electric field in the x_2-direction at the crystal surface, respectively.

The results of Equations 80 are complex numbers for varying depth d. In order to interpret these results the complex variation is changed to a magnitude and phase angle. Figures 3 and 4 show the variation of displacement and electric field amplitude as a function of depth d.

As discussed in a previous section the electric field of the piezoelectric surface wave exists outside the material as well as inside. This field has been analyzed with the results given in Table 2. Figure 4 also shows the variation of the external field, $\frac{E_2}{E_2(0)}$, as a function of d.

Phase variation for the displacement components is shown in Figure 5. This variation is quite similar to that of Figure 2 for the approximate technique. Electric field phase variation is plotted in Figure 6.

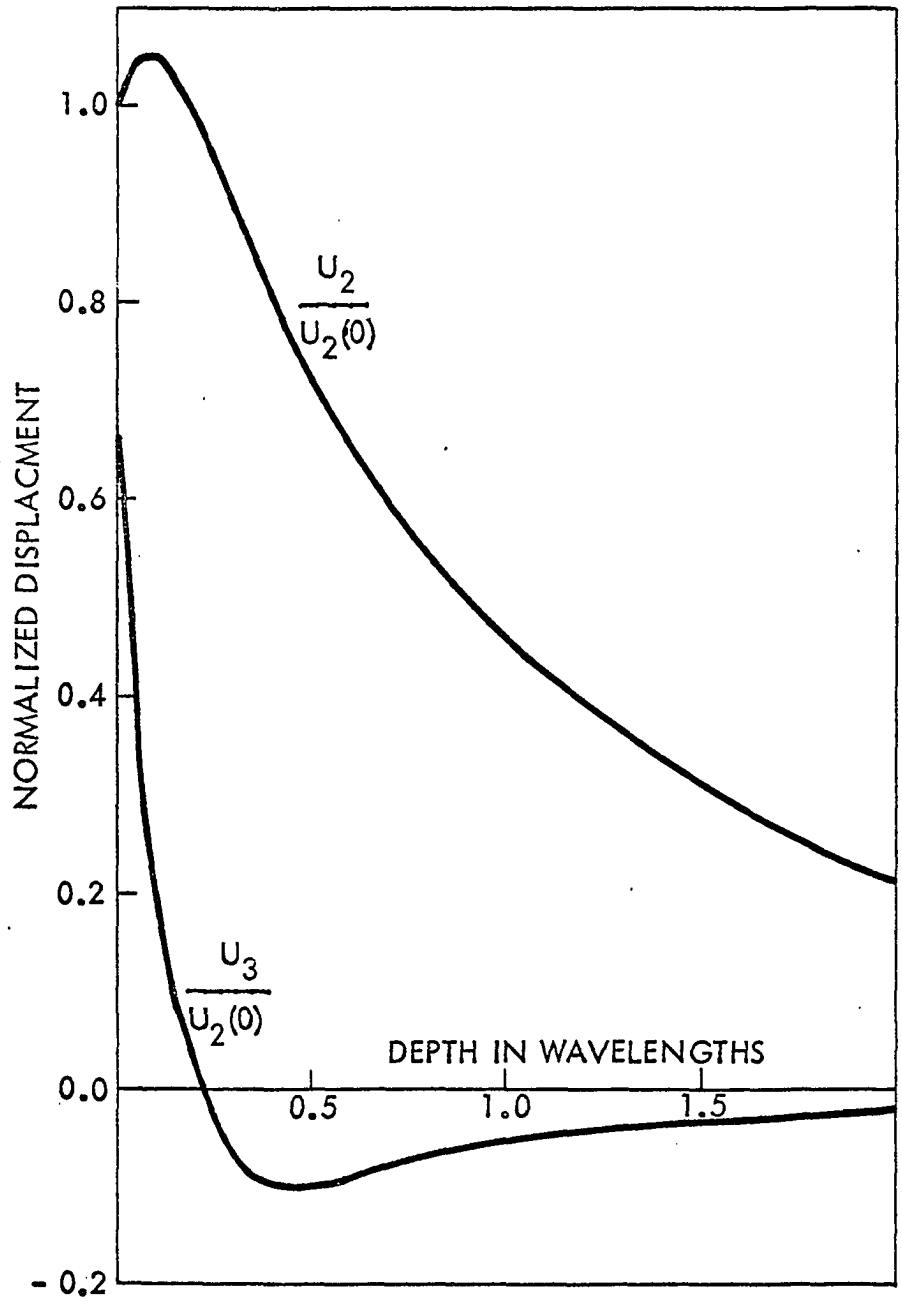

Figure 3. Normalized particle displacement versus depth for piezoelectric surface wave propagation on $LiNbO_3$

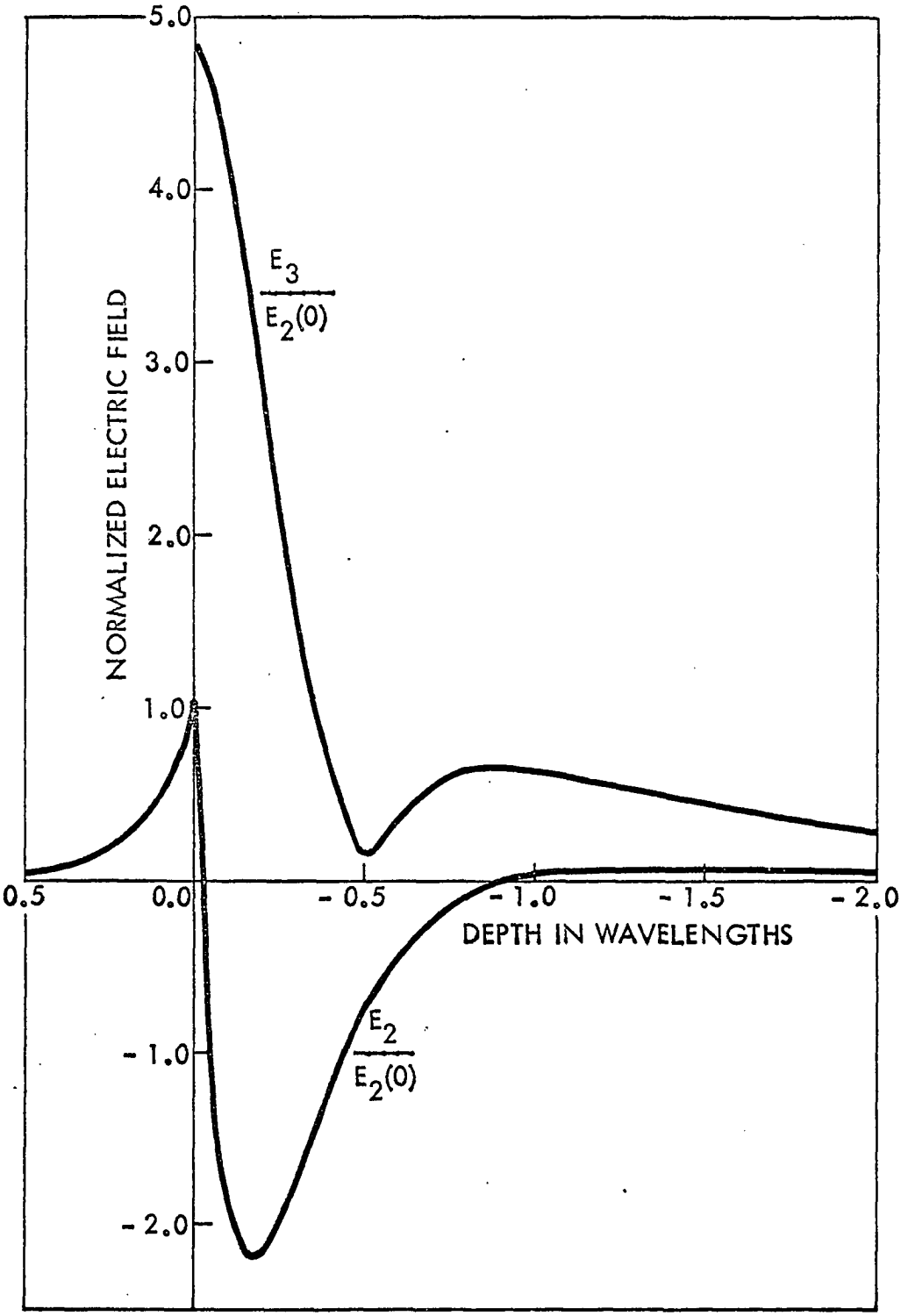

Figure 4. Normalized electric field intensity versus depth for surface wave propagation on $LiNbO_3$

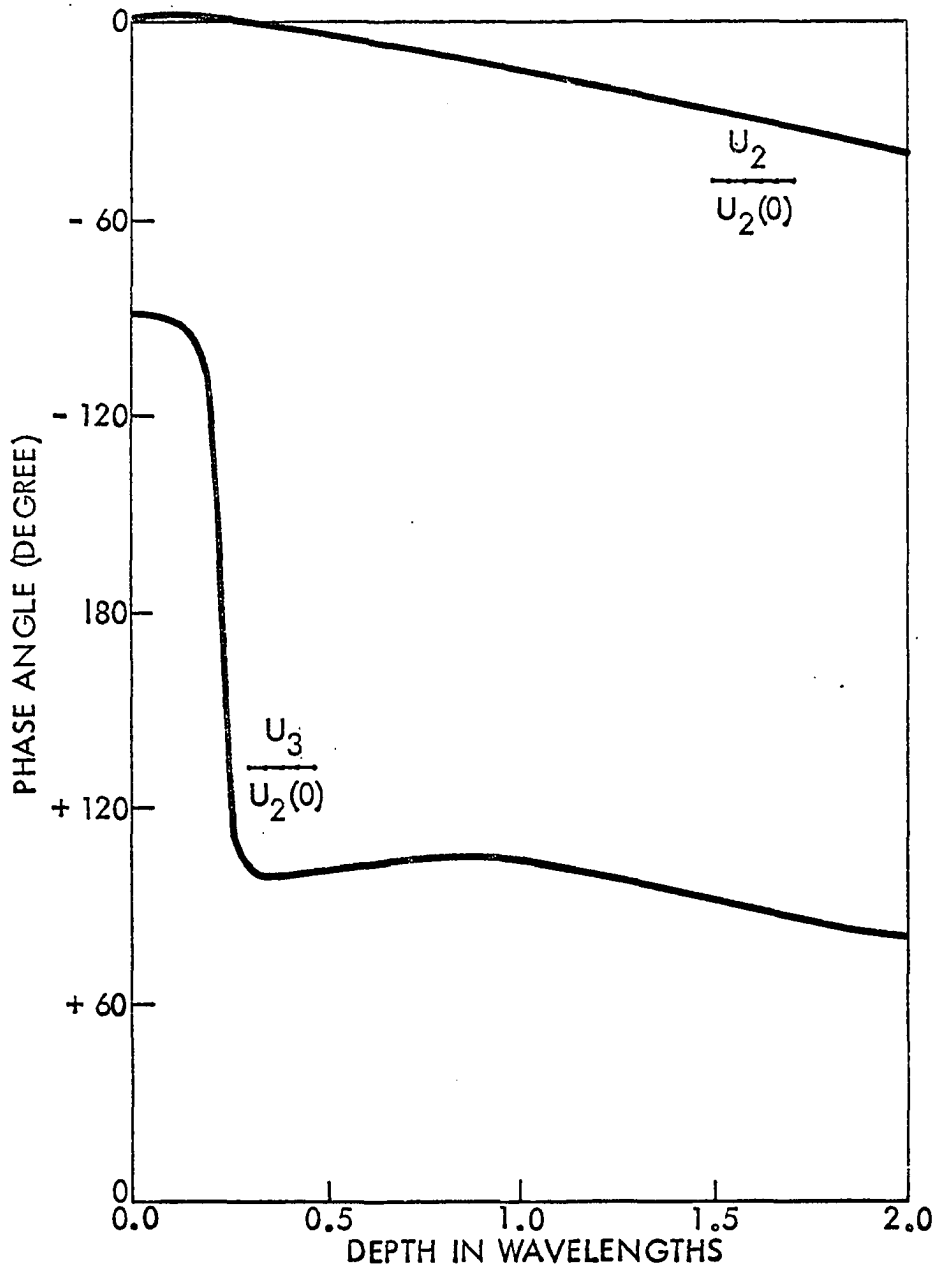

Figure 5. Phase relation of displacement components for piezoelectric surface wave propagation on $LiNbO_3$

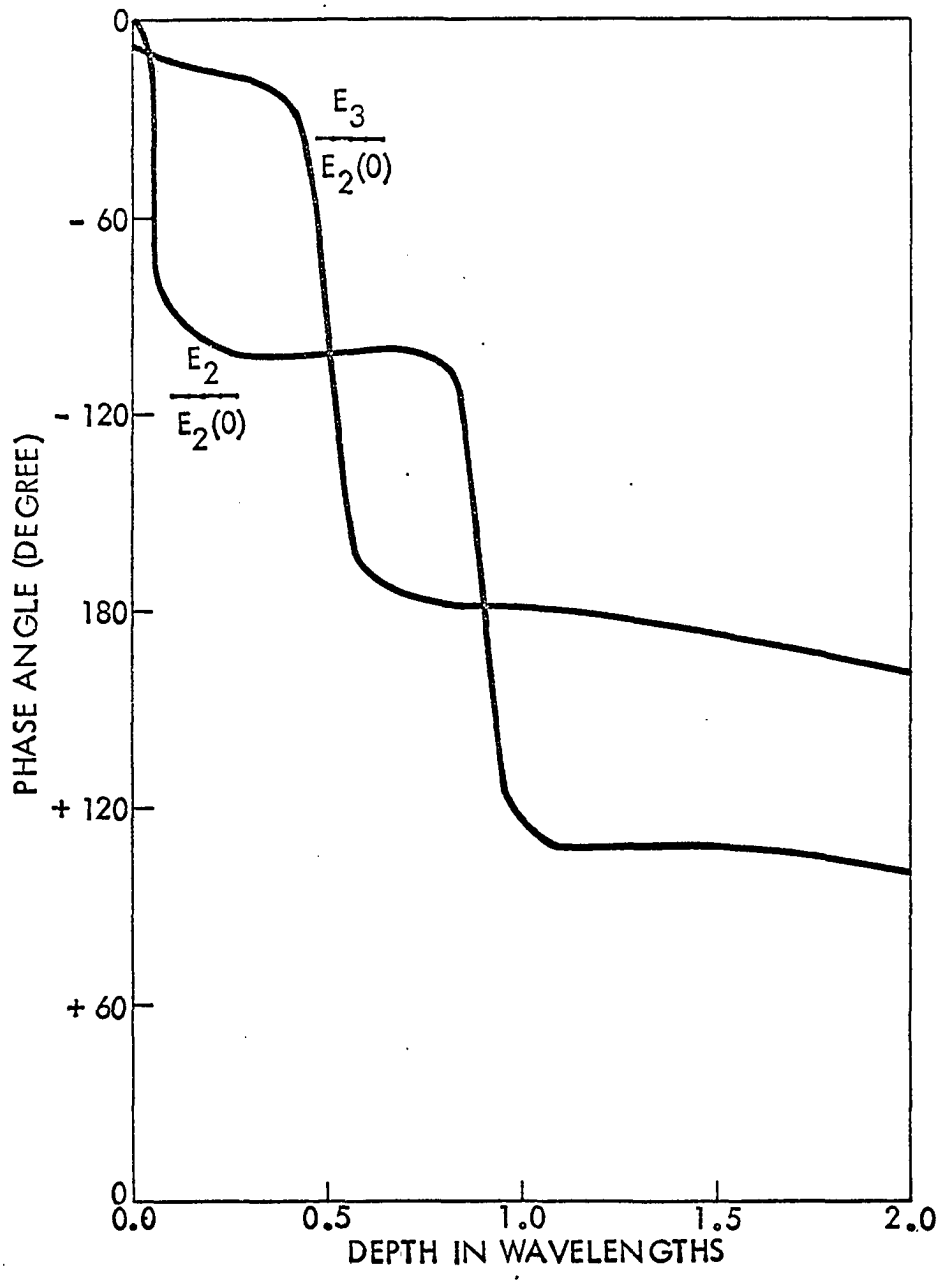

Figure 6. Phase relation of field components for surface wave propagation on $LiNbO_3$

III. THEORETICAL CONCLUSIONS

Rayleigh mode surface wave propagation has been shown to exist on $LiNbO_3$ crystals of the orientation discussed. These waves were analyzed by two methods. First the material was assumed nonpiezoelectric to form an approximation which simplified the problem considerably. A numerical technique was employed to determine the values of propagation velocity and corresponding decay constants which would simultaneously satisfy both the secular equation and the boundary conditions. A solution was found which produced the generalized Rayleigh mode of propagation.

The next method took the piezoelectric effect into account. The numerical technique was repeated and the generalized Rayleigh mode was again found.

Table 13 compares the results of these two methods. The resultant expressions for displacement amplitudes derived from the two methods differ radically in form. The result of these expressions, however, is quite similar as shown in Figure 7. Obviously no information regarding the electric field intensity inside the material can be gained from the approximate technique.

The major difference in the two methods is the propagation velocity. Piezoelectric coupling of the elastic wave to an electromagnetic wave increases the propagation velocity significantly in $LiNbO_3$. This result agrees with Tseng and

Table 13. Comparison of the approximate and the piezoelectric solutions

	Nonpiezoelectric approximation	Piezoelectric solution
Propagation velocity	3.3924×10^3 m./sec.	3.5105×10^3 m./sec.
Decay constants	$\alpha_1 = 0.08734 - i0.2297$	$\alpha_1 = 0.06462 - i0.1217$
	$\alpha_2 = -0.1431 - i1.3073$	$\alpha_2 = 0.03804 - i1.0379$
	$\alpha_3 = 0$	$\alpha_3 = -0.3960 - i0.7738$
Amplitude ratios	$n_1 = -0.0666 + i0.1614$	$n_1 = -0.5180 + i0.09719$
	$p_1 = 0$	$p_1 = (-1.5202 - i0.6931) \times 10^9$
	$o_1 = 0$	$o_1 = (0.2723 + i0.1945) \times 10^9$
	$m_{21} = -0.2947 - i0.1726$	$m_{21} = -0.02637 + i0.3719$
	$m_{31} = 0$	$m_{31} = 0.02740 - i0.5141$
	$n_{21} = -3.7549 + i0.4854$	$n_{21} = -1.9258 + i5.0940$
	$n_{31} = 0$	$n_{31} = -4.1163 - i1.4533$
	$o_{21} = 0$	$o_{21} = (-0.3243 - i0.2219) \times 10^2$
	$p_{21} = 0$	$p_{21} = (0.2723 + i0.1945) \times 10^2$
	$p_{31} = 0$	$p_{31} = -0.05632 + i5.3042$

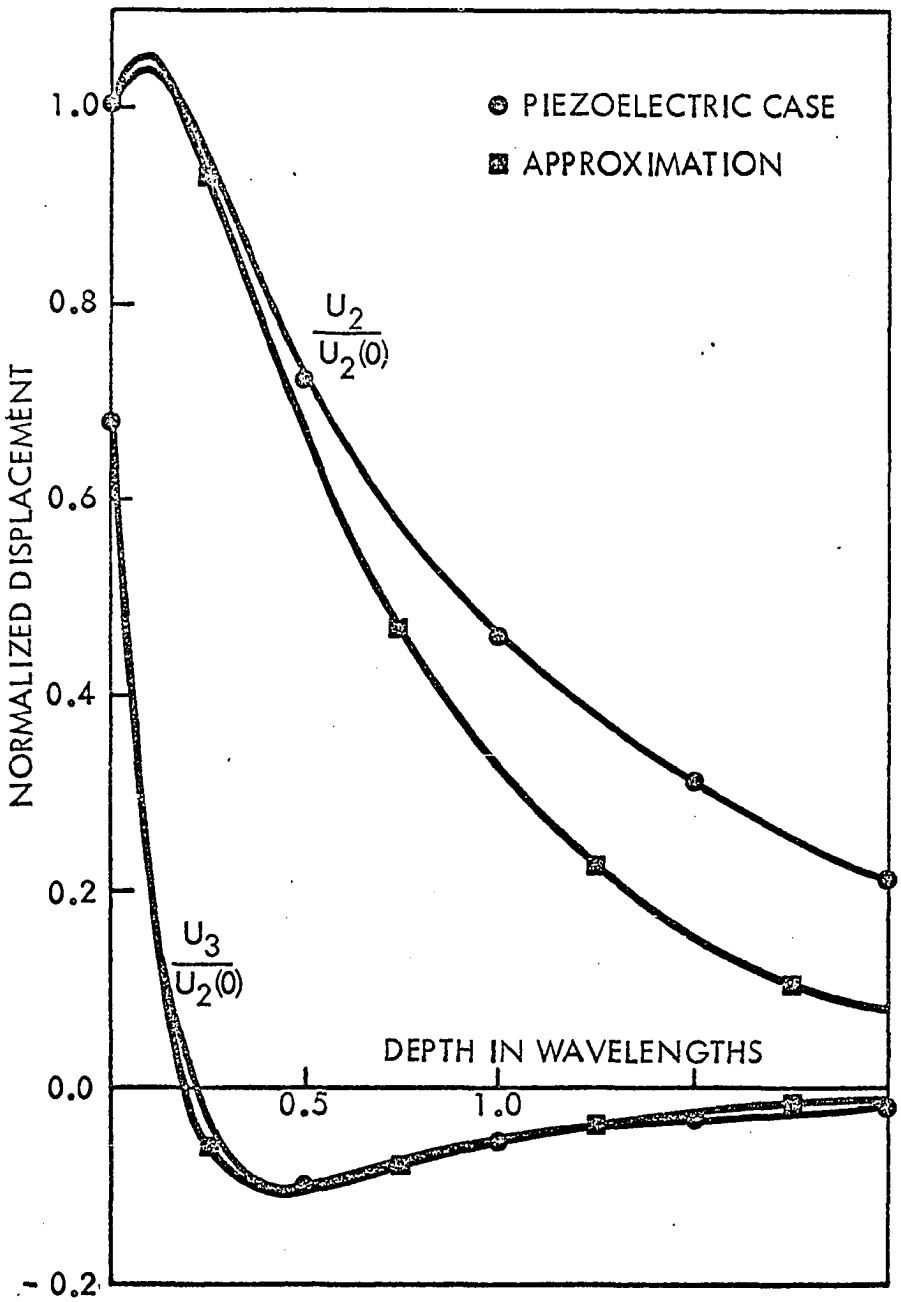

Figure 7. Comparison of particle displacements for the piezoelectric and approximate solutions

White's (15) analysis of hexagonal crystals. The analysis cited earlier by Campbell and Jones (1) indicated a velocity of approximately 3.49 x 10^3 m./sec., approximately 0.5% low compared to the 3.5105 x 10^3 m./sec. value obtained here.

IV. EXPERIMENTAL RESULTS

Results of the theoretical section indicate the existence of a Rayleigh mode of surface wave propagation on $LiNbO_3$ crystals. For this mode to exist propagation is in the X_3-direction and attenuation in the X_2-direction; this requires a crystal orientation as shown in Figure 8. The crystallographic axes, a, b, and c, are related to the cartesian coordinates, X_1, X_2 and X_3 according to the 1949 IRE Standard (7). Since this mode of propagation is confined to the surface of the crystal great care must be taken in the alignment and polishing of the propagation face of the crystal.

A single crystal of $LiNbO_3$ was obtained. The crystal was Y-cut with the Z-axis parallel to the long direction. The Z-axis was oriented parallel to the surface within six minutes. The surface was polished optically flat with a maximum dig and scratch of 2-3μ. These high tolerances are necessary for low loss acoustic propagation.

White and Voltmer (18) reported the direct piezoelectric coupling to surface elastic waves by interdigital electrodes, Figure 9, which produces a periodic electric field on the surface and permits piezoelectric coupling to a surface wave. Prior to this time transduction had involved the mechanical coupling of a compressional or shear wave transducer to the body. This method of transduction was very inefficient and suffered the disadvantage that pressure contact was required

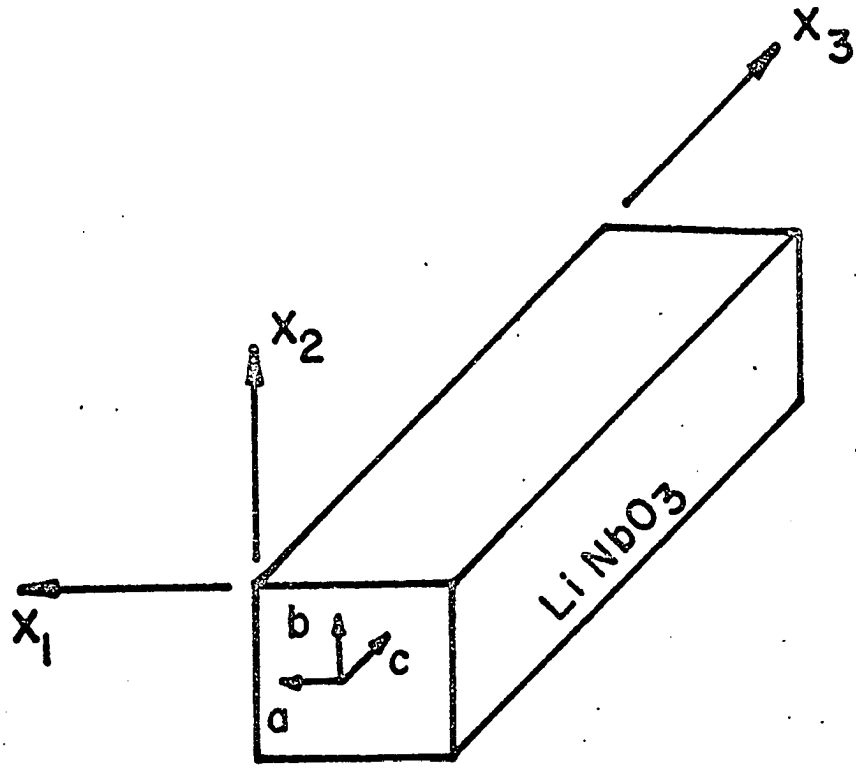

Figure 8. Orientation of crystallographic axes

Figure 9. Photograph showing one complete interdigital transducer

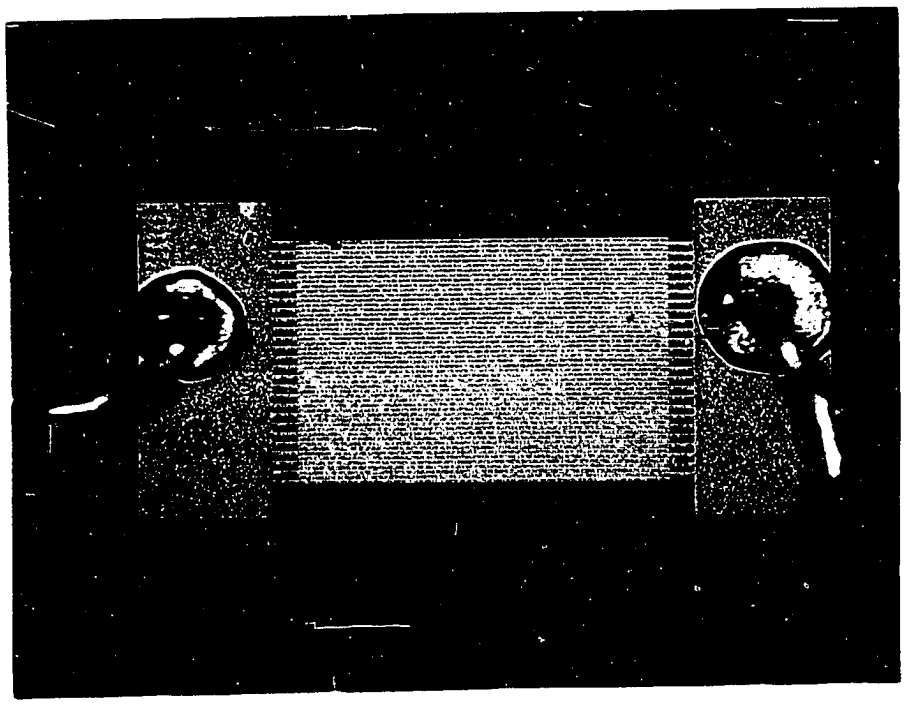

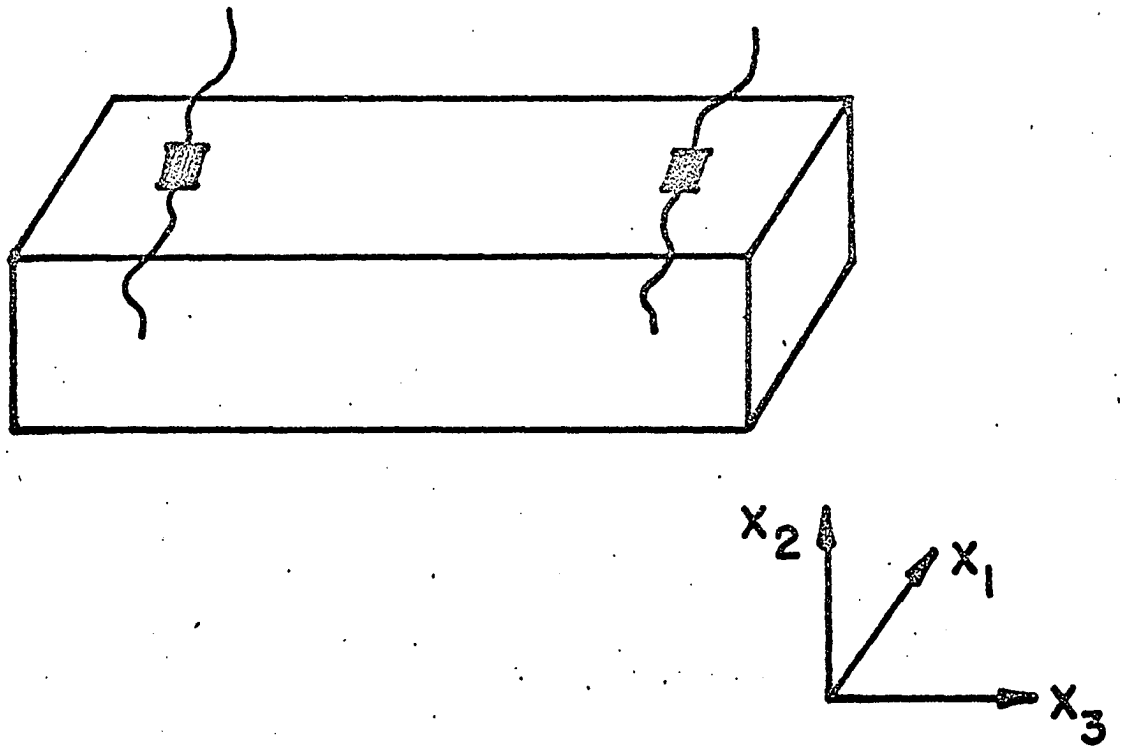

Figure 10. Orientation of transducers on $LiNbO_3$

which could easily damage the surface. Some of the advantages of this type of transducer are the extreme temperature range and the ability to increase the active transducer area by simply extending the electrode pattern in the direction of propagation.

The direct coupling to a surface elastic wave on the surface of a piezoelectric crystal is possible if any of the strain components at the surface is piezoelectrically active. For the $LiNbO_3$ crystal and orientation of the transducer shown in Figure 10, the S_6 components of strain is coupled piezoelectrically to the X_2 component of electric field, and the S_1 strain component is coupled to the X-component of field. Hence the r.f. field of electrode pattern is coupled directly to the displacement of the elastic wave, energy is transferred from the r.f. source to the elastic wave. The finger widths and spacings are made a quarter wavelength wide so that the period of the electrode pattern is equal to one wavelength of the desired frequency. The transducer will also operate at odd harmonics of the fundamental frequency.

Interdigital transducers were applied to each end of the crystal in the Z-direction. Each electrode contains 50 total fingers and occupied 0.1 inch including pads in the X-direction with an active region of 0.06 inches in the Z-direction. The fingers were evaporated over a photoetched mask. Aluminum was used as the electroding material with gold wires attached to the four pads. The transducers were

Figure 11. Photograph of a portion of one interdigital transducer showing details of electrical connection and fingers. Magnification is approximately 55:1.

Figure 12. $LiNbO_3$ crystal mounted in the plexiglass enclosure.

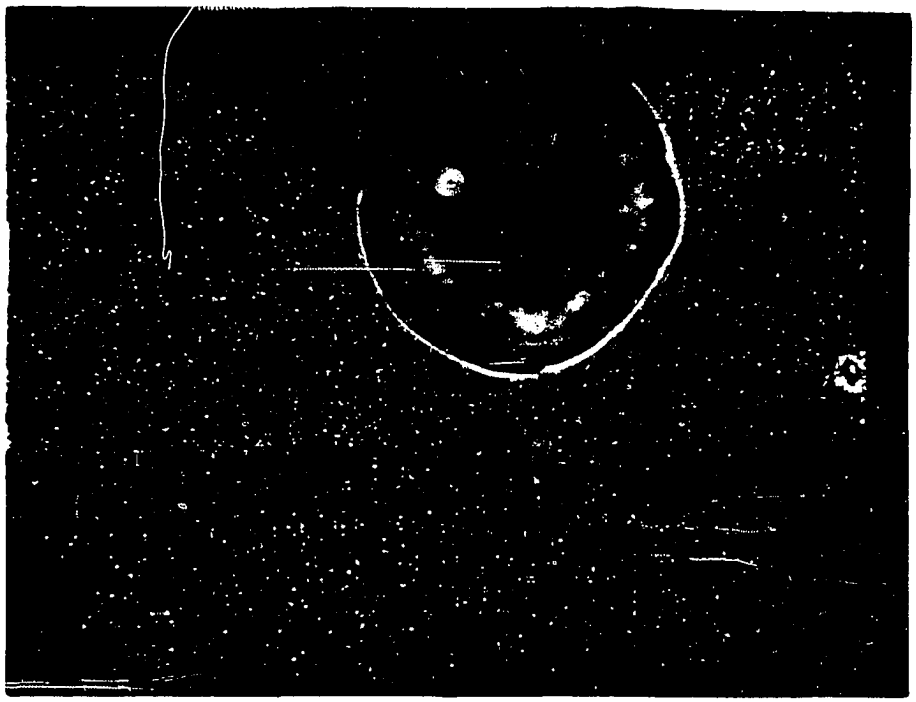

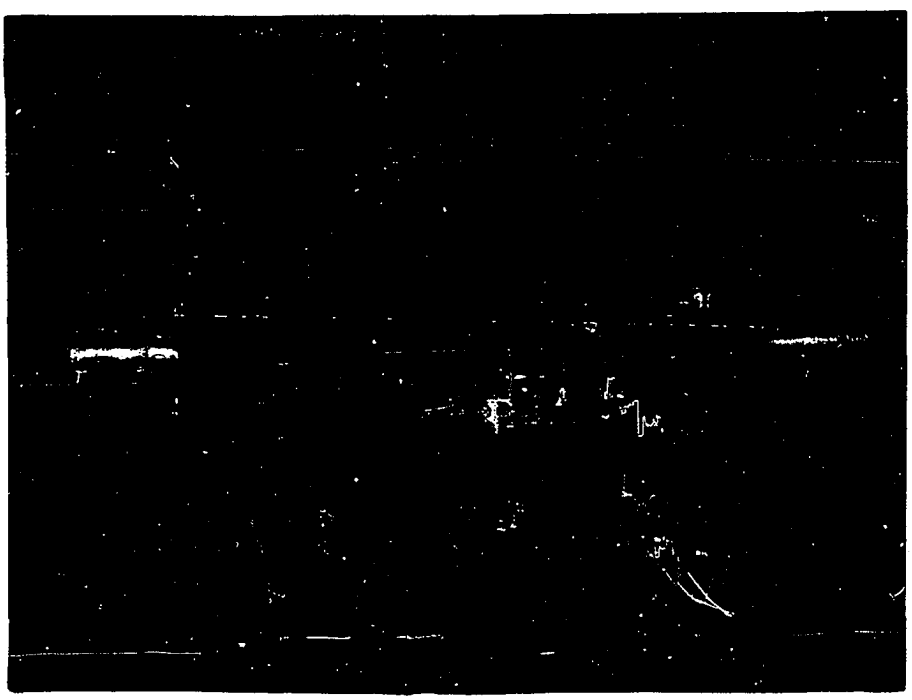

designed to operate at 100 MHz. A photo of a magnified portion of one of the transducers is shown in Figure 11.

Connection to the transducers is accomplished by a gold wire bonded to each electrode pad. These wires are in turn attached to coax connections on the ends of the plexiglass box constructed to protect the surface and transducers. The composite structure is shown in Figure 12.

A. Frequency Response of the Transducers

A theoretical analysis of the frequency response of interdigital transducers has been made by Tseng (14). His results indicate that the output amplitude increases as the total number of fingers N increases. Bandwidth decreases as N increases and is given approximately as

81 $$\Delta f = (\frac{2}{N}) f_0$$

where Δf is the frequency difference between half power points,

f_0 is the fundamental frequency,

N is the total number of fingers.

For the transducers used in this investigation the approximate bandwidth is found to be 3.28 MHz.

The experimental arrangement used to measure the frequency response is shown in Figure 13. The oscillator frequency was varied from 80 MHz to 330 MHz maintaining a

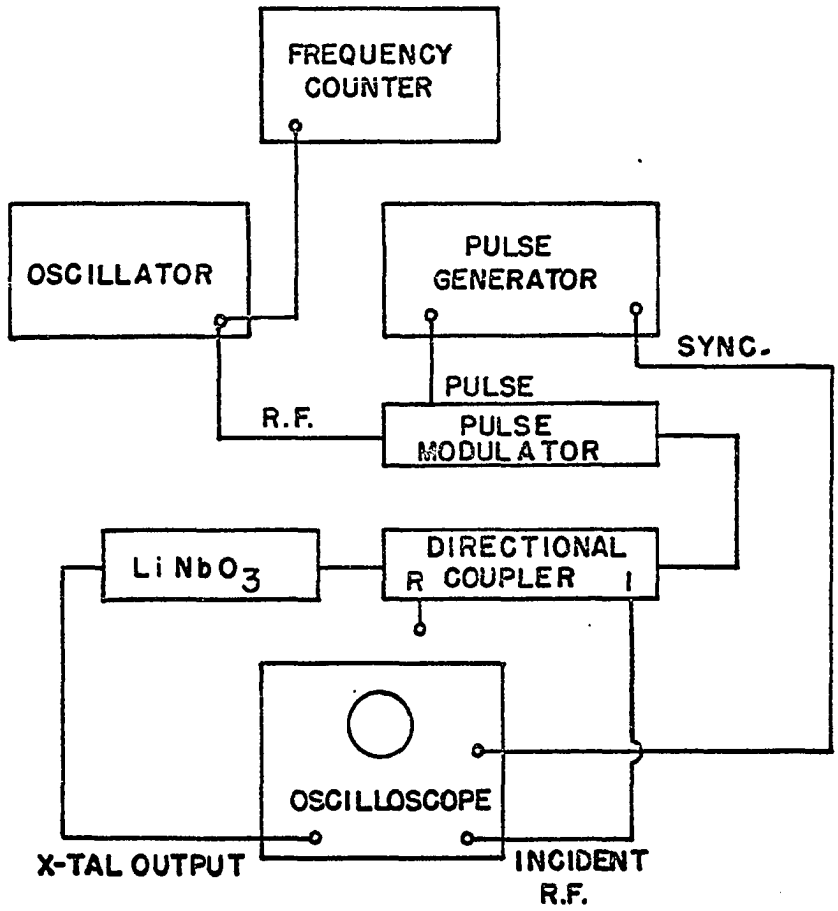

Figure 13. Experimental arrangement for measuring frequency response of the interdigital transducers

constant output power level. The crystal output was measured each megacycle. A magnitude plot for the entire range is shown in Figure 14 while detailed amplitude variations for the fundamental and third harmonic appear in Figures 15 and 16 respectively. Tseng plotted transducer response to the fundamental and third harmonic for a particular choice of width to space ratio of the fingers and a particular number of fingers N. The variation of fundamental response with number of fingers was also plotted for a range of 12 to 42 fingers. Extrapolation of these results to the electrodes used here indicates the form of response found agrees well with Tseng's theory.

The experimental bandwidth is found from Figure 15 to be 3.1 MHz which agrees very well with the theoretical value. Tseng indicates that the measured bandwidth for $LiNbO_3$ is found to be 20% less than the theory indicates. This is not the case here; theoretical and experimental results agree to within about 5.5%. The experimental bandwidth is less than the theoretical one, however, which does agree with Tseng.

Over all losses of the device were computed for operation at 104.5 MHz and 314 MHz; these losses include acoustic loss in the $LiNbO_3$ as well as transducer loss. These results are summarized below:

f(MHz)	Loss (db)
104.5	13
314	25

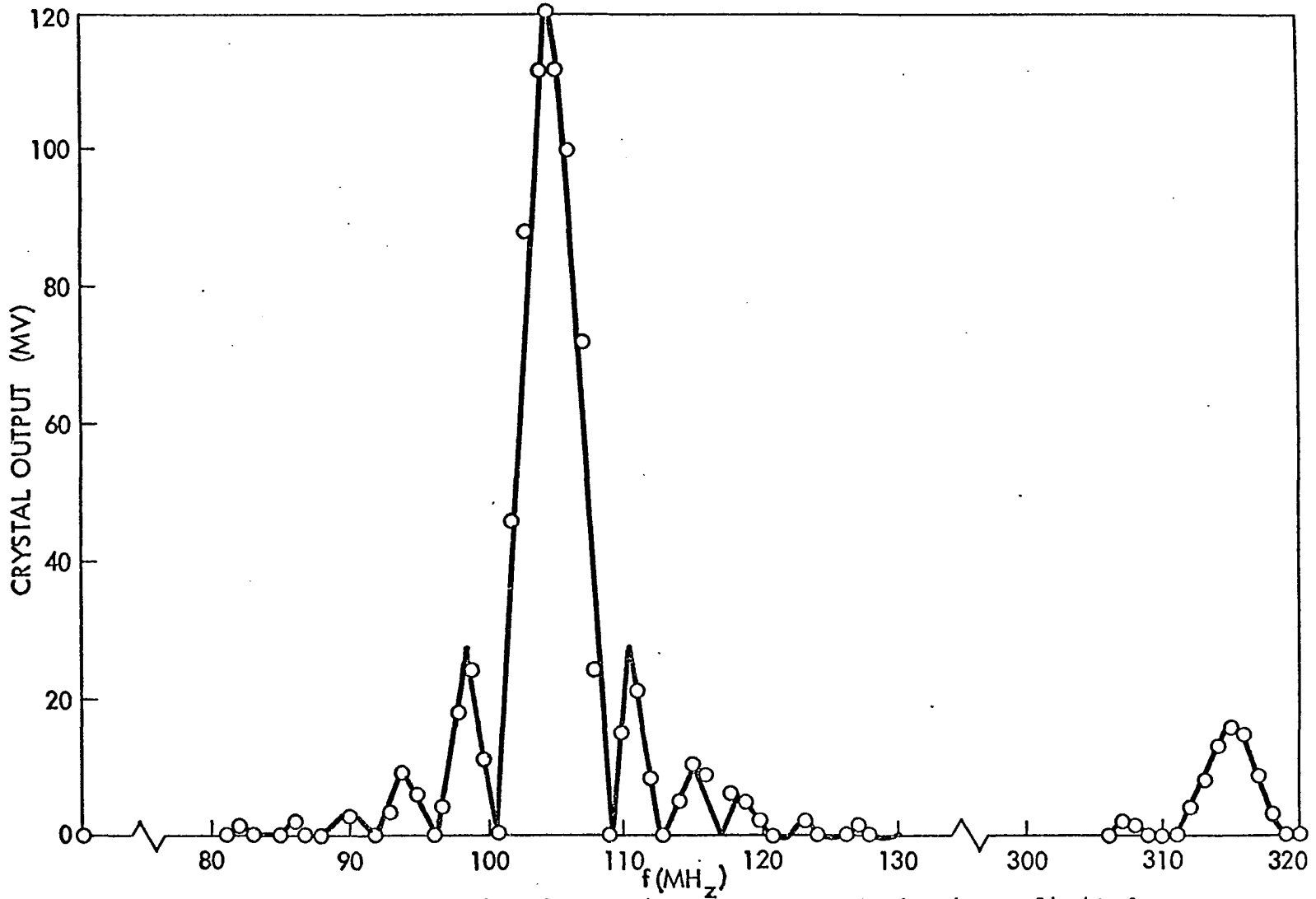

Figure 14. Fundamental and third harmonic response of the interdigital transducers

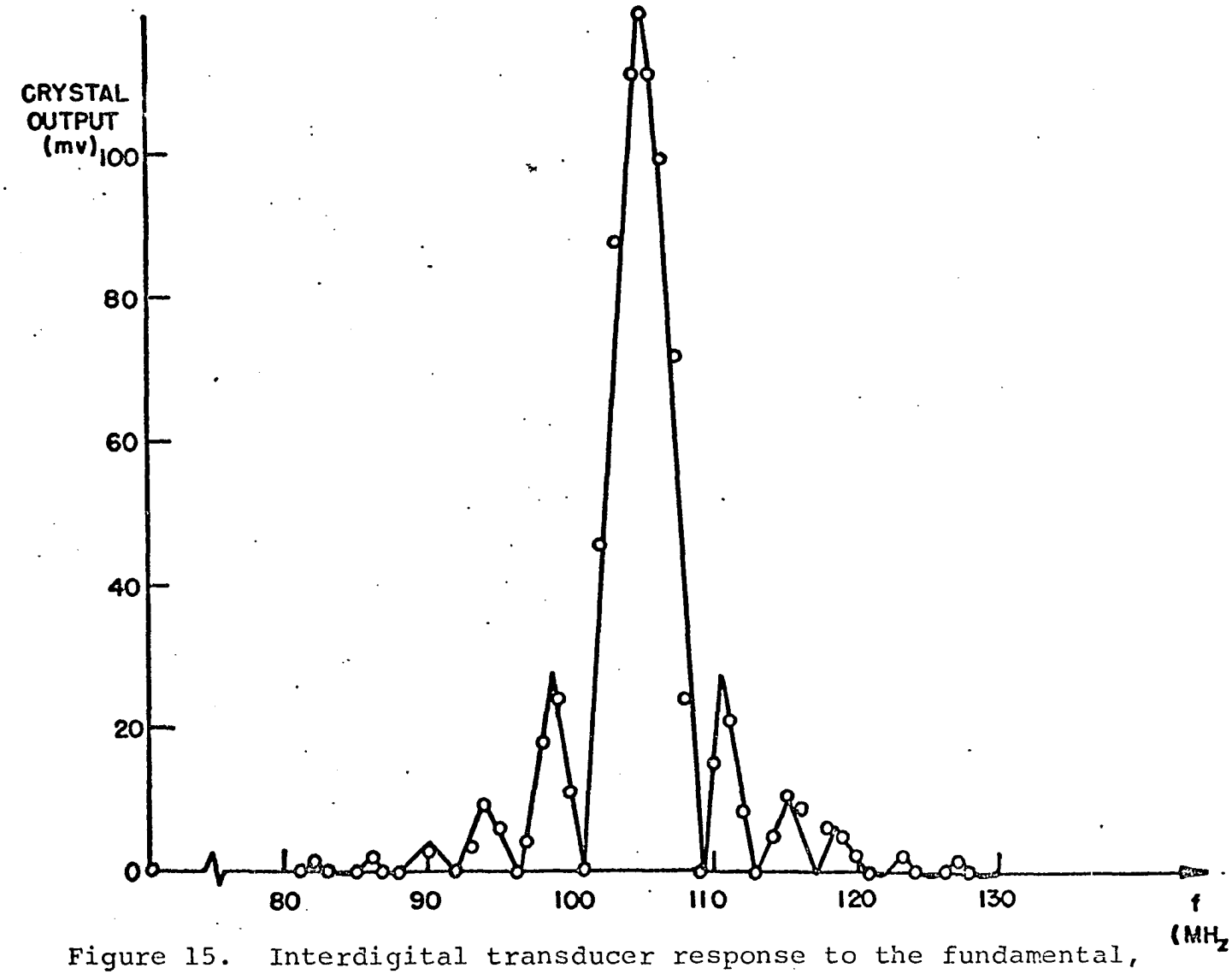

Figure 15. Interdigital transducer response to the fundamental, f = 105 MHz

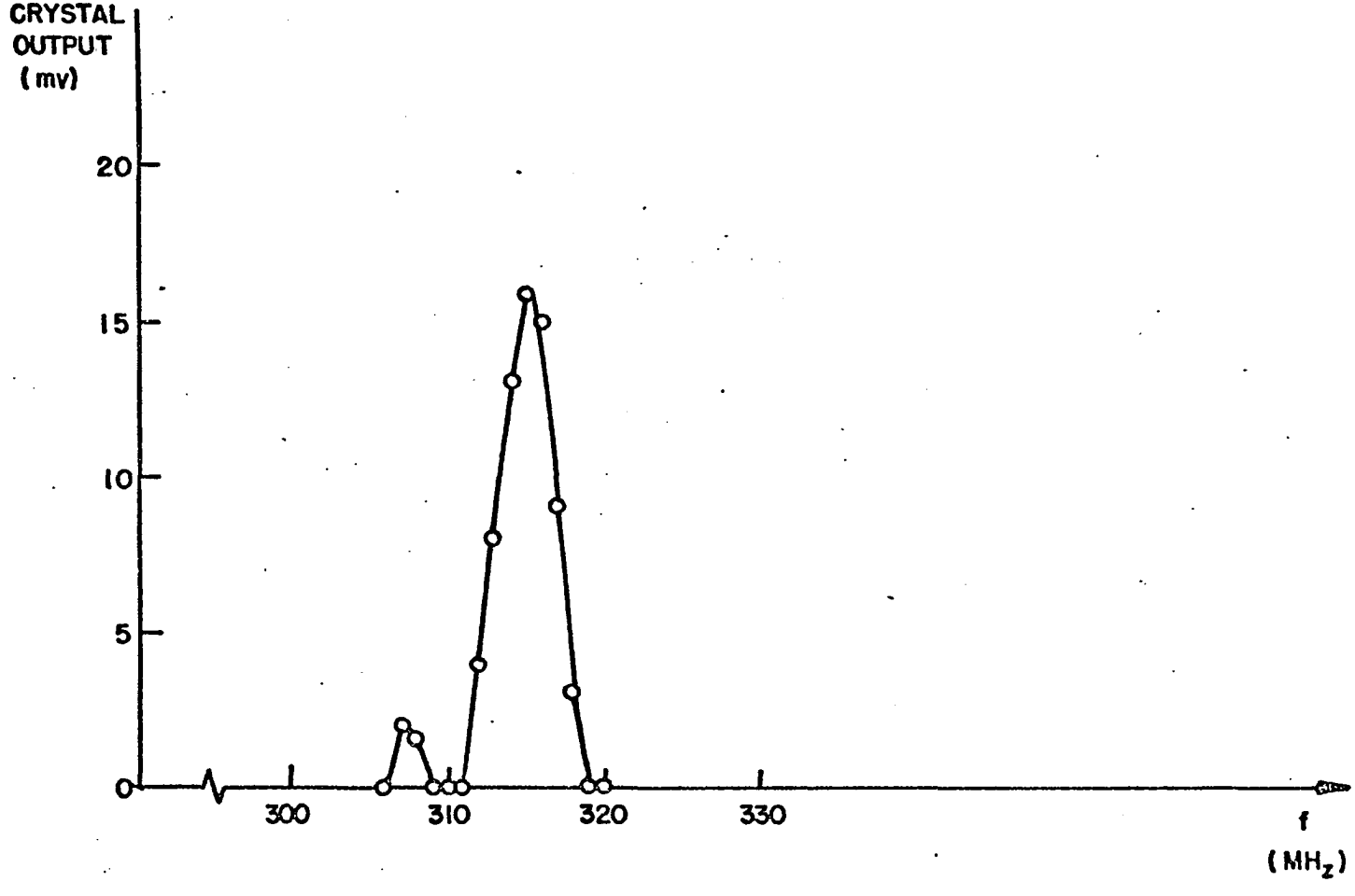

Figure 16. Interdigital transducer response to the third harmonic, f = 315 MHz

B. Delay Time Measurement

Propagation velocity is one of the main pieces of information determined in the theoretical section. To determine the validity of the theoretical calculations a measure of the propagation velocity was made on the $LiNbO_3$ crystal. A block diagram for the measurement technique appears in Figure 17. The r.f. oscillation is pulse modulated to produce 1 μsec. packets of r.f. energy. The pulses are propagated through a directional coupler and then through the crystal. The crystal output and incident r.f. wave are displayed on an oscilloscope and the time delay between them measured; the oscilloscope traces are shown in Figure 18 for an operation frequency of 105 MHz. The time delay was measured to be 3.9 μsec. which when divided into the electrode separation of 0.54 inches gives the experimental velocity as 3.52×10^5 cm./sec. Comparison of experimental and theoretical velocities appears in Table 14.

Table 14. Comparison of theoretical and experimental propagation velocities

	Nonpiezoelectric approximation	Piezoelectric calculation	Experimental
Propagation velocity ($\times 10^3$ m./sec.)	3.3924	3.5105	3.52

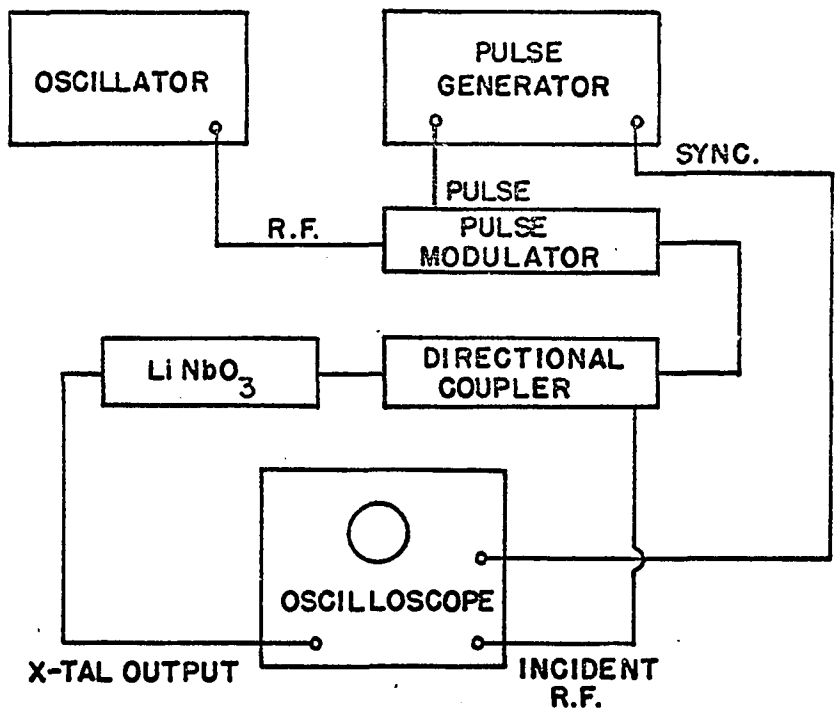

Figure 17. Experimental arrangement for measuring delay time

Figure 18. R.f. pulses showing time delay at a frequency of 315 MHz. Top trace is input signal out of a directional coupler (down ≈ 29 db), 10 mv/cm vertical sensitivity. Bottom trace is output of crystal with a 5 mv/cm vertical sensitivity. Horizontal scale is 1 μsec/cm.

Figure 19. R.f. pulses showing time delay at a frequency of 105 MHz. Traces same as Figure 18 except vertical sensitivity of bottom trace is 50 mv/cm.

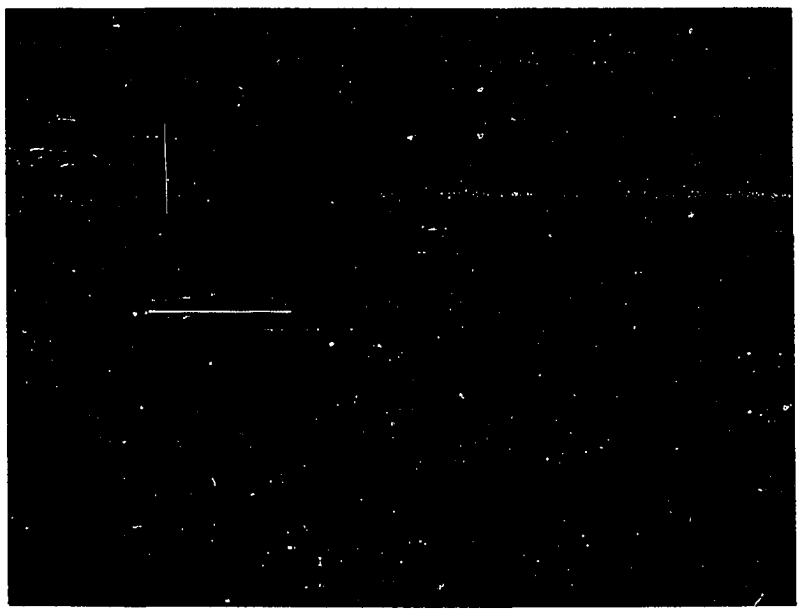

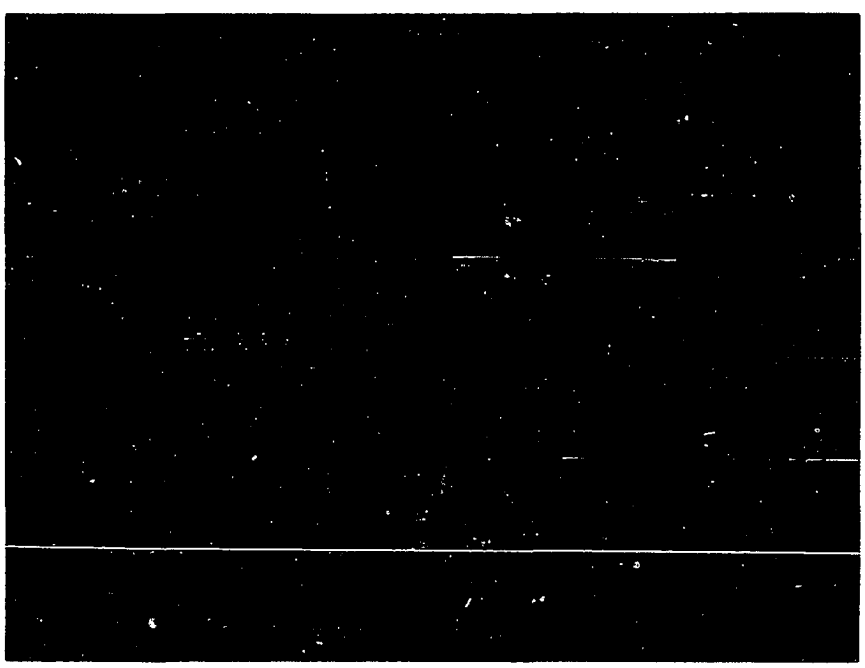

The theoretical development also predicted that the propagation velocity was independent of frequency. Operating at the third harmonic, 315 MHz, the measurement was repeated finding the delay time to again be 3.9 μsec. Figure 19 shows the oscilloscope traces for this case.

The small r.f. packet appearing to the right of the lower trace in Figure 19 is an echo from the output end of the crystal. Because the elastic waves do propagate on the surface these echoes can be easily removed by application of a soft absorber such as wax or rubber cement to the ends of the material. This was not done here because the danger of damaging the electrode connections presented a greater threat than the small echo.

V. LITERATURE CITED

1. Campbell, J. J. and Jones, W. R. A method for estimating optimal crystal cuts and propagation directions for excitation of piezoelectric surface waves. Institute of Electrical and Electronics Engineers Transactions on Sonics and Ultrasonics SU-15: 209-217. 1968.

2. Derewsiewicz, H. and Mindlin, R. D. Waves on the surface of a crystal. Journal of Applied Physics 28: 669-671. 1957.

3. Gazis, D. C., Herman, R. and Wallis, R. F. Surface elastic waves in cubic crystals. Physical Review 119: 533-544. 1960.

4. Gold, L. Rayleigh wave propagation on anistropic (cubic) media. Physical Review 104: 1532-1536. 1956.

5. Koerber, G. G. Propagation of piezoelectric surface waves. Iowa State University of Science and Technology Engineering Research Institute Report 437. 1969.

6. Love, A. E. H. Some problems of geodynamics. London, England, University Press. 1911.

7. Mason, W. P. Crystal physics of interaction processes. New York, N.Y., Academic Press. 1966.

8. Nassau, K., Levinstein, H. J. and Loiacono, G. M. Ferromagnetic lithium niobate. 2. Preparation of single domain crystals. Journal of Physics and Chemistry of Solids 27: 989-996. 1966.

9. Rayleigh, Lord. On waves propagated along the plane surface of an elastic solid. London Math Society Proceedings 17: 4-11. 1885.

10. Stoneley, R. The propagation of surface elastic waves in a cubic crystal. Royal Society (London) Proceedings A232: 447-458. 1955.

11. Stoneley, R. The seismological implications of aeolotropy in continental structure. Geophysical Supplement to Monthly Notes, Royal Astronomical Society 5: 343. 1949.

12. Synge, J. L. Elastic waves in anisotropic media. Journal of Mathematics and Physics 35: 323-334. 1957.

13. Tseng, C. C. Elastic surface waves on free surface and metalized surface of CdS, ZnO, and PZT-4. Journal of Applied Physics 38: 4281-4284. 1967.

14. Tseng, C. C. Frequency response of an interdigital transducer for excitation of surface elastic waves. Institute of Electrical and Electronics Engineers Transactions on Electron Devices ED-15: 586-594. 1968.

15. Tseng, C. C. and White, R. M. Propagation of piezoelectric and elastic surface waves on the basal plane of hexagonal piezoelectric crystals. Journal of Applied Physics 38: 4274-4280. 1967.

16. Warner, A. W., Onoe, M. and Coquin, G. A. Determination of elastic and piezoelectric constants for crystals in class (3m). Journal Acoustical Society of America 42: 1223-1231. 1967.

17. White, R. M. Surface elastic-wave propagation and amplification. Institute of Electrical and Electronics Engineers Transactions on Electron Devices ED-14: 181-189. 1967.

18. White, R. M. and Voltmer, F. W. Direct piezoelectric coupling to surface elastic waves. Applied Physics Letters 7: 314-316. 1965.

19. Wylie, C. R. Advanced engineering mathematics. 2nd ed. New York, N.Y., McGraw Hill Book Co., Inc. 1960.

VI. ACKNOWLEDGMENTS

The author wishes to express his appreciation to Dr. G. G. Koerber for his help and guidance throughout the research and to Dr. R. E. Post for his many helpful discussions and suggestions. The author also wishes to express his appreciation to Mr. Bud Meador and Mr. Michael White for their assistance in writing the digital computer programs.

Financial support for this investigation was provided by Project Themis, A Center of Excellence in Ceramic and Composite Materials, Contract No. F33615-68-C-1034, Project No. 713-S.

VII. APPENDIX

Solution of the transverse mode requires the simultaneous solution of the secular equation

$$(-v^2\rho + 2C_{14}\alpha + C_{66}\alpha^2 + C_{44})(\mu_0 v^2 \varepsilon_{11} - \alpha^2 - 1) + \mu_0 v^2 (e_{15} - e_{22}\alpha)^2 = 0 \qquad \text{A1}$$

and the boundary conditions given by Equations 41 and 45 as

$$\begin{vmatrix} (C_{14} + \alpha_1 C_{66} + e_{22} m_1) & (C_{14} + \alpha_2 C_{66} + e_{22} m_2) \\ (\alpha_1 - \beta) m_1 & (\alpha_2 - \beta) m_2 \end{vmatrix} = 0. \qquad \text{A2}$$

For a pure transverse mode to exist requires the decay constants to be negative imaginary numbers. If α is replaced by $-ir$ where r is a root of the secular equation which given a pure mode the secular equation becomes a quartic equation in r with real coefficients on even powers of r and imaginary coefficients for the odd powers. By the definition of a pure mode and the choice of $-ir$ for α, the r's in the modified secular equation are necessarily real and positive. Replacing α by $-ir$ in Equation A1 gives

$$(-v^2\rho - i2C_{14}r + C_{66}r^2 + C_{44})(\mu_0 v^2 \varepsilon_{11} + r^2 - 1) + \mu_0 v^2 (e_{15} + ie_{22}r)^2 = 0. \qquad \text{A3}$$

Expansion of Equation A3 yields a complex polynomial in r. For this equation to be satisfied requires that both the real and imaginary components are individually satisfied. The following equations are the real and imaginary parts of Equation A3 respectively and must both be true,

A4a
$$(-v^2\rho - C_{66}r^2 + C_{44})(\mu_0 v^2 \varepsilon_{11} + r^2 - 1) + \mu_0 v^2 (e_{15}^2 - e_{22}^2 r^2) = 0$$

A4b
$$-2C_{14}r(\mu_0 v^2 \varepsilon_{11} + r^2 - 1) + 2\mu_0 v^2 e_{15} e_{22} r = 0.$$

The imaginary part of the secular equation, Equation A4b, gives r as (assuming $r \neq 0$)

A5
$$r = \pm \left(\frac{\mu_0 v^2 e_{22} e_{15} + C_{14}(1 - \mu_0 v^2 \varepsilon_{11})}{C_{14}}\right)^{\frac{1}{2}}.$$

Equation A5 indicates only one possible value of r which meets the requirements of a pure mode, real and positive. Hence the pure transverse mode reduces to a mode with degenerate roots. Boundary conditions for the case of a mode with degenerate roots are found to be

A6a
$$(C_{14} + \alpha_1 C_{66} + e_{22} m_1) = 0$$

A6b
$$(\alpha_1 - \beta) m_1 = 0$$

where α_1 is the acceptable root determined from Equation A5 and m_1 is the amplitude ratio as defined by Equation 39. Equation A6b indicates α_1 must equal β to satisfy these conditions. β, the decay constant outside the material, is given by Equation 20 to be

A7 $$\beta = + i\{1 - (\frac{v}{v_0})^2\}^{\frac{1}{2}}.$$

β is seen to be positive and imaginary, unacceptable for α. The pure transverse mode is therefore not possible in trigonal crystals of the orientation considered here.